OPEN ACCESS Freely available online

PLOS ONE

RIG-I Self-Oligomerization Is Either Dispensable or Very Transient for Signal Transduction

Jade Louber[1], Eva Kowalinski[2,3¤], Louis-Marie Bloyet[1], Joanna Brunel[1], Stephen Cusack[2,3], Denis Gerlier[1]*

1 Centre International de Recherche en Infectiologie, INSERM, U1111, CNRS, UMR5308, Université Lyon 1, ENS Lyon, Lyon, France, **2** European Molecular Biology Laboratory, Grenoble Outstation, Grenoble Cedex 9, France, **3** Unit of Virus Host-Cell Interactions, UJF-EMBL-CNRS, UMI 3265, Grenoble Cedex 9, France

Abstract

Effective host defence against viruses depends on the rapid triggering of innate immunity through the induction of a type I interferon (IFN) response. To this end, microbe-associated molecular patterns are detected by dedicated receptors. Among them, the RIG-I-like receptors RIG-I and MDA5 activate IFN gene expression upon sensing viral RNA in the cytoplasm. While MDA5 forms long filaments *in vitro* upon activation, RIG-I is believed to oligomerize after RNA binding in order to transduce a signal. Here, we show that *in vitro* binding of synthetic RNA mimicking that of *Mononegavirales* (Ebola, rabies and measles viruses) leader sequences to purified RIG-I does not induce RIG-I oligomerization. Furthermore, in cells devoid of endogenous functional RIG-I-like receptors, after activation of exogenous Flag-RIG-I by a 62-mer-5′ppp-dsRNA or by polyinosinic:polycytidylic acid, a dsRNA analogue, or by measles virus infection, anti-Flag immunoprecipitation and specific elution with Flag peptide indicated a monomeric form of RIG-I. Accordingly, when using the *Gaussia* Luciferase-Based Protein Complementation Assay (PCA), a more sensitive *in cellula* assay, no RIG-I oligomerization could be detected upon RNA stimulation. Altogether our data indicate that the need for self-oligomerization of RIG-I for signal transduction is either dispensable or very transient.

Citation: Louber J, Kowalinski E, Bloyet L-M, Brunel J, Cusack S, et al. (2014) RIG-I Self-Oligomerization Is Either Dispensable or Very Transient for Signal Transduction. PLoS ONE 9(9): e108770. doi:10.1371/journal.pone.0108770

Editor: Pierre Boudinot, INRA, France

Received June 3, 2014; **Accepted** September 4, 2014; **Published** September 26, 2014

Funding: This work was supported by grant from FINOVI foundation and ANR (CARDINNATE grant). The funders had no role in study design, data collection and analysis, decision to publish, or preparation of the manuscript.

Competing Interests: The authors have declared that no competing interests exist.

* Email: denis.gerlier@inserm.fr

¤ Current address: Max Planck Institute for Biochemistry, Martinsried, Germany

Introduction

In vertebrates, the first step of innate immunity is the detection of microbe-associated molecular patterns (MAMPs) by specific pattern-recognition receptors (PRRs) [1,2]. RIG-I (retinoic acid-inducible gene I) belongs to the cytoplasmic RIG-I-like receptors (RLRs) together with MDA5 (melanoma differentiation-associated protein 5) and LGP2 (laboratory of genetics and physiology 2). In response to infection by RNA viruses, RIG-I activates type-1 interferon (IFN) genes [1,3,4,5,6]. RIG-I consists of two amino-terminal caspase activation and recruitment domains (CARDs) that are essential for signal transduction, a central helicase and a C-terminal domain both of which bind an agonist RNA. The mechanism of RIG-I activation has been widely studied over the past few years. RIG-I preferentially recognizes 5′-triphosphorylated (5′ppp) blunt ended double-stranded RNA, but it can also bind to long double-stranded RNA (dsRNA) without 5′ppp [7,8,9,10]. The recognition of an agonist RNA triggers a conformational change, allowing RIG-I to become active thanks to the release of the CARD domains. The free CARDs are then accessible for poly-ubiquitination and recruitment of the adaptor mitochondrial antiviral signal (MAVS) protein [1,11,12,13].

The precise mechanisms of RIG-I activation are still not fully understood. It has been proposed that RIG-I-mediated activation relies on RIG-I oligomerization via dimerization of RIG-I C-terminal domain (CTD), multiple oligomerization sites within RIG-I, and/or RNA-mediated oligomerization [7,10,14,15,16,17,18,19,20,21]. In the present study, we question the necessity of RIG-I self-oligomerization for signal induction. RIG-I oligomerization, induced by synthetic cognate RNA able to activate RIG-I and as well as activation by measles virus (MeV), was analysed by co-immunoprecipitation and a sensitive protein complementation assay. In the absence of convincing evidence of self-oligomerization our data support monomeric RIG-I as being the minimal signal transduction unit.

Materials and Methods

Cells and virus

Huh7.5 [22], Vero [23] and 293T [24] cells were maintained in Dulbecco's modified Eagle's medium (DMEM Gibco, Invitrogen) supplemented with 10% foetal calf serum (Gibco), 10 mM HEPES, 2 mM L-glutamine, 10 μg/ml gentamycine and 1% non-essential amino acids for Huh7.5 cells at 37°C and 5% CO_2.

Moraten-eGFP measles virus was recovered by reverse genetics as described by Radecke et al. [25]. The helper cell line 293-3-46 stably expressing T7 polymerase, MeV N and P proteins [25] was transfected using the ProFection kit (Promega) with plasmids coding for MeV genome with an additional eGFP gene and MeV-L protein (pEMCLa). Three days after transfection, cells were

overlaid on Vero cells. Upon appearance, isolated syncytia were picked and individually propagated on Vero cells. Virus stock was produced after a second passage at multiplicity of infection (MOI) 0.03 on Vero cells. Virus was checked for lack of mycoplasma contamination, sequence accuracy and infectivity (virus titration).

Plasmids

Wild-type human RIG-I and RIG-I^{ko} (T55I, Q229A, T697A, E702A, K888A, K907A) cDNA were subcloned into pEF-BOS expression vector using PCR amplification of cDNA fragments and in vitro recombination (InFusion, Clontech). HA, Cl25 (Ghannam et al., 2008) and Flag tag coding sequences were fused to RIG-I cDNA during the PCR amplification step. RIG-I insert constructs were entirely verified by sequencing (Eurofins).

The two original expression vectors used for *Gaussia* Luciferase-Based Protein Complementation Assay (PCA) (Cassonnet et al., 2011), were modified into pCI-glu1 and pCI-glu2 to eliminate the Gateway insert without changing the flanking vector sequence in order to preserve the linker bridging glu domains and inserts. HA-RIG-I and Cl25-RIG-I fragments were subcloned upstream or downstream of gaussia glu1 and/or glu2 domains by InFusion recombination of PCR-amplified fragments. Gcn4 sequence [26] was subcloned upstream or downstream of RIG-I coding sequence by InFusion recombination of PCR-amplified fragments. All plasmids were verified by sequencing of every subcloned PCR fragment.

Antibodies and reagents

For immunoblotting the following primary antibodies were used: anti-Flag (1:1,000; M2, Sigma), Cl25 anti-MeV N (1:1,000) [27], anti-HA (1:1,000; Clone HA-7, Sigma), 49.21 anti-MeV P (1:2,000) [28] anti-GAPDH (1:2000; Millipore) murine monoclonal antibodies and anti-human RIG-I (1:10,000) rabbit polyclonal antibodies [29].

For DNA plasmid transfection, JetPRIME reagent (Polyplus transfection) was used in 293T cells and Transit-LT1 reagent (Mirus) was used in Huh7.5 cells. RNA transfection was performed with Oligofectamine reagent (Invitrogen). Poly(I:C) was purchased from Amersham Biosciences.

Rabies leader 5′ppp-RNA (GGACGCUUAACAACAAAAC-CAGAGAAGAAAAAGACAGCGUCAAUUGCAAAC-GAAAAAUGUGC), measles leader 5′ppp-RNA (GGACCAAA-CAAAGUUGGGUAAGGAUAGAUCAAUCAAUGAU-CAUAUUCUAGUACACUUGAAUUC) and Ebola leader 5′ppp-RNA (GGACACACAAAAAGAAAGAAAA-GUUUUUUATACUUUUUGUGUGCGAAUAACUAUG) were *in vitro* T7 transcribed and purified by excising the band after denaturing urea-PAGE [30].

The 62-mer-5′ppp-dsRNA was obtained by annealing two T7 transcribed and purified complementary 62-mer-5′ppp-ssRNA (GGUCCUGUCUGUUGUCGGUCUCGUUUGUUGCGU-GUCCGUGUUCGCCUUGGUUCCCCGGUGCC) and (GGCACCGGGGAACCAAGGCGAACACGGACACGCAA-CAAACGAGACCGACAACAGACAGGACC). Both 62-mer-5′ppp-ssRNA were made from only three nucleotides to avoid secondary structure and preclude T7 polymerase re-initialization on and copy of the nascent RNA [31].

SEC MALLS

Purified recombinant human RIG-I was prepared as previously described [30] and mixed with equimolar amounts of RNA. Experiments were performed in 20 mM HEPES, pH 7.5, 100 mM NaCl, 2.5 mM MgCl2, 5 mM β-mercaptoethanol with an S200(10/300) column, connected to a MALLS detector (DAWN-EOS Wyatt technology) and a refractive index detector (RI2000b Schambeck). Data were analysed with the ASTRA V software [32].

SAXS

The experiments were carried out at the beamline ID14-2 of the European Synchrotron Radiation Facility (ESRF, Grenoble, France). Scattering data was collected for different protein concentrations and from the merged curves the radius of gyration (Rg) was determined from the Guinier plot. Next, the maximal distance in the size distribution function was adjusted, so the calculated Rg from the fit would be in agreement with the experimental value.

Luciferase assay

Cells were seeded into 96-well plates and, 18 h later, transfected with 50 ng DNA of IFN-β luciferase, 17 ng DNA of renilla luciferase and 33 ng DNA of RIG-I plasmid. One day after DNA transfection, cells were transfected with Poly(I:C), synthetic RNA or infected with Moraten-gfp virus at MOI 1. The following day, the luciferase assay was performed using the Dual-Glo system from Promega. Firefly luciferase values were normalized to renilla luciferase to measure transfection efficiency.

For *Gaussia* Luciferase-Based Complementation Assay (PCA) [33], cells were seeded into 96-well plates and, 8 h later, transfected with 100 ng RIG-I-glu1 construct and 100 ng RIG-I-glu2 construct. Twenty four hours after DNA transfection, cells were transfected or not with Poly(I:C). Eighteen hours later, the luciferase assay was performed using the Renilla Luciferase Assay System (Promega). Protein-protein interaction levels were expressed in normalized luminescence ratio (NLR) according to the following formula:

$$\mathrm{NLR} = (\text{glu1-A} + \text{glu2-B})\ \text{signal} \Big/ [(\text{glu1-A} + \text{glu2})\ \text{signal} + (\text{glu1} + \text{glu2-B})\ \text{signal}],$$

where glu1-A and glu2-B are the chimeric proteins, and glu1 and glu2 the empty vector coding only for the glu fragment.

Immunoprecipitation and immunoblot analysis

For immunoblot analysis, transfected or infected cells were suspended in lysis buffer, either PLB buffer (10 mM HEPES pH 7.4, 100 mM NaCl, 5 mM $MgCl_2$, 0.05% NP-40, 25 mM EDTA) or NP-40 buffer (50 mM Tris HCl pH 7.4, 150 mM NaCl, 0.1% NP-40, 1 mM EDTA) both complemented with Complete (Roche) protease inhibitor cocktail for 20 minutes on ice. The proteins were then separated from cell debris by centrifugation at 7,000×g for 10 minutes. Proteins were denatured by addition of Laemmli 1X buffer and heating at 100°C for 3 minutes before analysis by SDS-PAGE and immunoblotting.

For co-immunoprecipitation analysis, lysates were incubated from 2 h to 16 h at 4°C on a rotating wheel with anti-Flag (M2) beads (Sigma). Beads were washed four times with lysis buffer and proteins were eluted by addition of 22.5 µg 3xFlag Peptides (Sigma). Lysates were then analysed by SDS-PAGE and immunoblotting.

RNA extraction and amplification

RNA immunoprecipitated with RIG-I was purified by Trizol/chloroform extraction, then amplified by stem-loop RT-PCR as set up for miRNA detection [34] using the Reverse Transcriptase Superscript^{TM} II from Invitrogen and the Taq Polymerase from New England Biolabs. Stem-loop primer used for retrotranscrip-

tion of measles leader RNAs was GCGACGTTCCGTTGCGATCAGCGTACGCTGATCGCAACGGAACGTCGCcatagt and PCR primers were accaaacaaagttgggtaagg and GCTGCTACTCGGCTGATCTCAC.

Results

Oligomer state of RIG-I:RNA complexes formed *in vitro*

The ability of human RIG-I (hRIG-I) protein to bind different 5′ppp RNA *in vitro* was tested by Multi-Angle Laser Light Scattering coupled to Size Exclusion Column (SEC-MALLS) analysis. Purified recombinant hRIG-I was able to bind to synthetic copies of the leader RNAs from three different *Mononegavirales* families: Ebola (*Filoviridae*), rabies (*Rhabdoviridae*) and measles (*Paramyxoviridae*) viruses (Figure 1A). The incubation of hRIG-I with each synthetic leader RNA induced a shift to a lower elution volume which indicates a larger, more elongated or less globular particle. This observation points to a conformational change of the protein molecule: either the addition of the RNA moiety to one end of the protein elongates the whole complex, or large parts of bound RNA are flexible and floppy. However, when looking at the apparent molecular masses from MALLS, none of the complexes showed a significant mass shift. RIG-I alone appeared with a mass of 100 kDa, slightly smaller than the calculated mass of 106 kDa, but within the error range. RIG-I associated with the leader RNA of Ebola, rabies or measles virus appeared with a mass of 102 kDa, 110 kDa and 113 kDa, respectively. Moreover, the resulting complex was monodispersed (one peak, flat MALLS signal). It can be concluded that RIG-I binds to each of these RNAs and forms a homogeneous complex with a 1:1 stoichiometry. When examined by Small Angle X-Ray Scattering (SAXS) the radius of gyration R_g for RIG-I without RNA appears to be 38.5±0.27 Å and with a short panhandle RNA of influenza virus to be slightly larger 42.2±0.21 Å. This represents an elongation of the molecule but no dimerization. P(R) functions of the scattering curves (Figure 1B) that were fitted to attain the experimental R_g both show a maximal intramolecular distance of 150 Å. The curve of apo RIG-I clearly flattens out around 100 nm, corresponding to the dimensions observed for various crystal structures while the curve of RNA-bound RIG-I accumulates larger distances between 100 nm and 150 nm, probably due to the release of the CARDs.

RIG-I binding to synthetic RNA *in cellula* and activation of IFN-β promoter

Since RNA sensing by RIG-I results in IFN-β gene expression, the ability of the synthetic RNAs to induce the expression of a luciferase reporter gene under the control of the IFN-β promoter was tested. To avoid any interference of the endogenous innate immune response of the host cell, we selected Huh7.5 cells since they lack TLR3 and MDA5 expression, express a defective T55I RIG-I mutant and exhibit a poor feedback upregulation of RLR genes due to an IFNAR signalling defect [7,35,36,37,38]. In cells transiently expressing Flag-RIG-I (Figure 2A), the 62-mer-5′ppp-dsRNA was the best RIG-I stimulator, whereas the 62-mer-5′ppp-ssRNA induced only minimal luciferase activity (Figure 2B). While rabies leader (RabV-L) RNA was almost as good an activator of RIG-I as the 62-mer-5′ppp-dsRNA, the Ebola (EboV-L) and measles (MeV-L) leader RNAs induced intermediate and lower responses, respectively (Figure 2B). Rabies, Ebola and measles leader RNAs were T7-transcribed and purified by denaturing urea-PAGE. However, double-stranded side products cannot be totally avoided with this technique [9,10,39] and may explain their ability to activate RIG-I in the same way as the 62-mer-5ppp-dsRNA. It is also possible that these RNA could adopt different secondary structures enabling them to activate RIG-I. Alternatively, they can hybridize to cellular RNA since blasting their 5′ppp extremities revealed several >13 nt long complementary RNA transcribed sequences present in the human genome, although none have been identified as being enriched in RNA bound to RIG-I from measles virus infected cells [40].

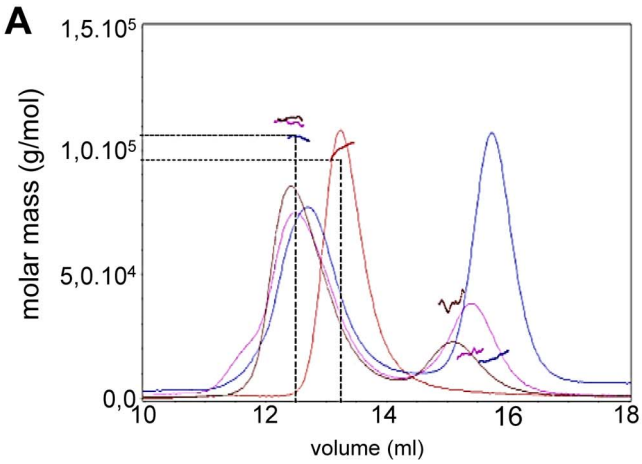

	RIG-I:RNA	Free RNA
RIG-I	100±7%	
RIG-I + EboV-L	102±3%	15±47%
RIG-I + RabV-L	110±7%	18±30%
RIG-I + MeV-L	113±7%	39±47%

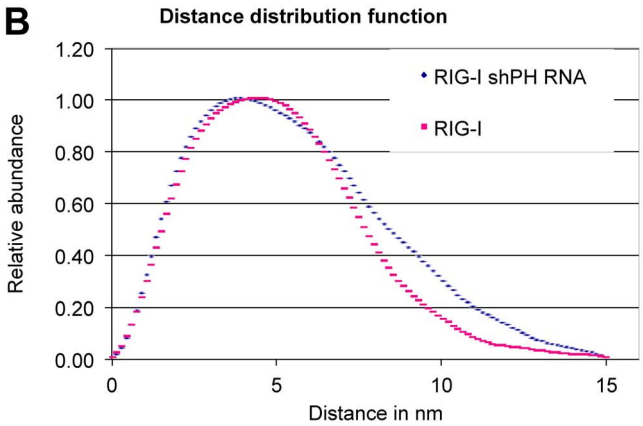

Figure 1. Oligomeric state of RIG-I:RNA complexes produced *in vitro* as determined by SEC MALLS (A) and SAXS (B). (A) 37 mM RIG-I and RIG-I:RNA complexes formed by incubation with 40 mM of RNA and 2 mM ATP analogue were analysed by size-exclusion chromatography on a S200 column coupled to multi-angle laser light scattering. Free RIG-I as well as the RIG-I:RNA complex elutes as monomers or 1:1 complexes, respectively, with indicated apparent molecular weights. Theoretical values are 106 kDa for RIG-I and 11.8 kDa for the RNA. (B) Scattering data was collected for different protein concentrations of RIG-I or RIG-I:RNA complex and from the merged curves. shPH RNA is an influenza virus derived short pan-handle RNA. The radius of gyration (R_g) was determined from the Guinier plot. P(R) functions of the scattering curves that were fitted to attain the experimental R_g show both a maximal intramolecular distance of 150 Å.
doi:10.1371/journal.pone.0108770.g001

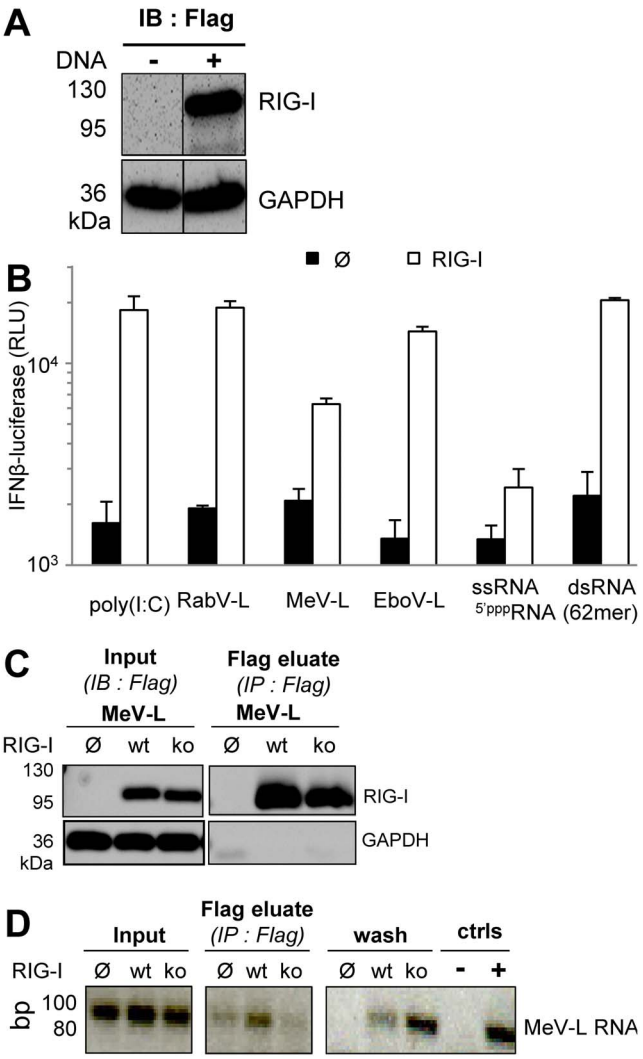

Figure 2. RIG-I binding to synthetic RNA and activation of IFN-β promoter. (A) Expression of Flag-RIG-I in Huh7.5 cells two days after transfection and analysed by western blot as revealed with Flag-specific antibody. (B) Luciferase expression driven under the control of the IFN-β promoter measured 24 h after transfection with 20 ng of synthetic RNA in Huh7.5 cells expressing or not Flag-RIG-I. (C, D) Immunoprecipitation of RIG-I:RNA complexes formed *in cellula*. Synthetic RNA were transfected in Huh7.5 cells previously transfected or not with Flag-RIG-I or Flag-RIG-I^{ko} 24 h before. Cells were harvested 6 hours after RNA transfection and RIG-I:RNA complexes were eluted from anti-Flag antibody immobilized on beads with a Flag peptide. (C) Specific immunoprecipitation of Flag-RIG-I as analysed by western blot. (D) RNA immunoprecipitated with Flag-RIG-I and analysed by RT-PCR.
doi:10.1371/journal.pone.0108770.g002

Measles leader RNA was also tested for its ability to form *in cellula* complexes with RIG-I that are stable enough to be detected by immunoprecipitation of RIG-I. This synthetic RNA was transfected in Huh7.5 cells expressing wild type RIG-I or a RIG-I^{ko} construct associating a T55I mutation in the first CARD domain (inhibition of TRIM25 recruitment) with Q229A, T697A, E702A and K888/907A mutations in the helicase and CTD that prevent RNA binding to the corresponding domain [41,42,43]. Measles leader RNA was recovered in detectable amounts from eluted wt RIG-I, but not from its RNA-binding deficient RIG-I^{ko} counterpart (Figure 2C, D). This data is in agreement with the enrichment in leader RNA sequences found in complex with RIG-I from measles virus infected cells [40].

Search for RNA induced RIG-I oligomerization *in cellula*

To determine whether RNA binding can induce RIG-I oligomerization *in cellula*, we built two expression vectors coding for RIG-I tagged with either Flag or Cl25 peptide. These constructs were expressed equally well as shown by similar signal in western blot revealed by anti-RIG-I antibodies (Figure 3 A). When expressed in Huh7.5 cells, both Flag-RIG-I and Cl25-RIG-I were stimulated by Poly(I:C) in a dose-dependent manner (Figure 3B) as expected from their strong expression levels (Figure 3A, C). To evaluate RIG-I oligomerization *in cellula*, Huh7.5 cells were co-transfected with Flag-RIG-I and Cl25-RIG-I constructs, stimulated by either Poly(I:C) or RNA transfection and finally harvested 18 hours after stimulation for an analysis in a co-immunoprecipitation assay. Cl25-RIG-I could not be co-immunoprecipitated with Flag-RIG-I, since similar trace amounts were detected in the absence or presence of RNA stimulation in Flag-RIG-I eluates (Figure 3C). Notably, Cl25-RIG-I could also not be co-immunoprecipitated with Flag-RIG-I after the transfection of the 62-mer-5′ppp-dsRNA although it has been shown to induce RIG-I dimerization *in vitro* (see Figure S3 in [30]).

Since we did not observe any RIG-I oligomerization *in cellula* after stimulation by Poly(I:C) or synthetic dsRNA, we tried to stimulate RIG-I by infecting cells with measles virus [42]. Huh7.5 cells were tested for their permissiveness to infection by Moraten-eGFP, a measles virus vaccine strain coding for eGFP as a viral reporter gene. Huh7.5 cells were infected by this virus as efficiently as were Vero cells that are commonly used for stock virus production (Figure S1 in File S1). We then tested the ability of measles virus infection to induce RIG-I oligomerization. Huh7.5 cells were co-transfected with Flag-RIG-I and Cl25-RIG-I, then infected or not with Moraten-eGFP virus and 18 hours later submitted to the immunoprecipitation assay. Both Flag-RIG-I and Cl25-RIG-I were strongly expressed (Figure 3D, inputs), but once again, we did not observe any detectable increase in the trace amounts of Cl25-RIG-I co-immunoprecipitated with Flag-RIG-I upon MeV infection (Figure 3D). We can exclude any pitfall in our procedures: the anti-Flag immunoprecipitation and elution procedure was well suited to detect the co-immunoprecipitation of N and P proteins from a recombinant MeV (Figure S2 in File S1) in agreement with the previously described interaction of these two proteins [44,45,46,47,48].

Since La Crosse virus (LACV) nucleocapsids that exhibited a triphosphorylated 5′ (5′ppp) terminus as does MeV can be co-immunoprecipitated with RIG-I from infected cells [49], we searched for any co-immunoprecipitation of the abundant MeV N protein with Flag-RIG-I, but none could be detected (Figure 3D). Incidentally, this observation confirms that 5-ppp (anti)genomic RNA from MeV cannot interact with RIG-I in physiological conditions likely because there are entirely covered by N protein as previously rationalized [42,50].

RIG-I oligomerization was also tested in 293T cells stimulated by transfection of Poly(I:C), synthetic dsRNA or ssRNA, or Moraten-eGFP infection and 18 hours later submitted to the immunoprecipitation assay. Both Flag-RIG-I and Cl25-RIG-I were strongly expressed (Figure 3E, inputs). This time, detectable amounts of Cl25-RIG-I were found in the Flag-RIG-I eluate. However, this was observed whether Poly(I:C), 5′ppp-dsRNA or 5′ppp-ssRNA was co-transfected with RIG-I (Figure 3E), and independently of their ability to activate the IFN-β promoter (Figure 3B). Moreover, after transfection of only a 1/20th amount of RNA, the amount of Cl25-RIG-I found in the anti-Flag

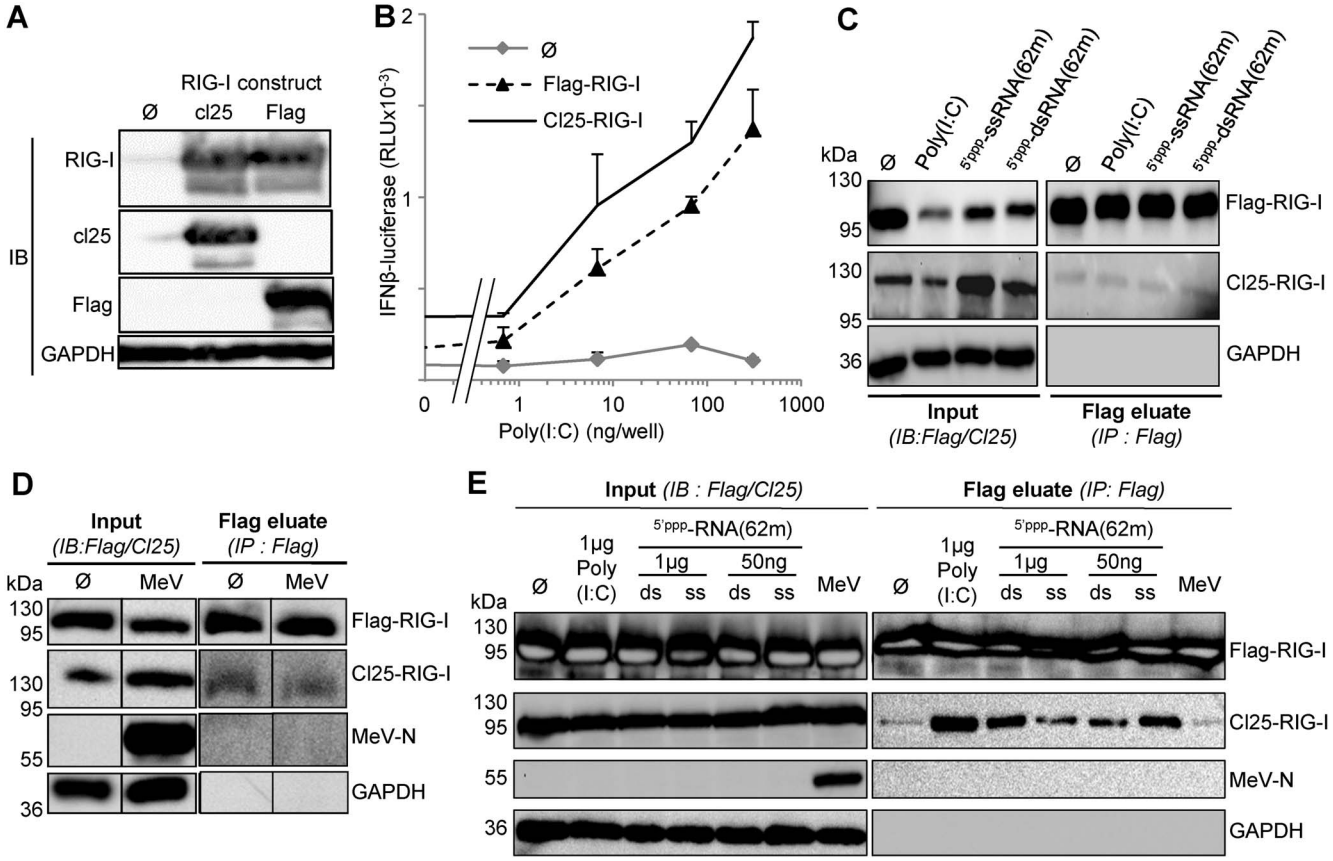

Figure 3. Analysis of RIG-I oligomerization *in cellula* as determined by co-immunoprecipitation 18 hours after stimulation by a cognate RNA ligand. (A) Similar expression of Flag-RIG-I and cl25-RIG-I constructs in 293T cells as revealed by western blot. (B) Efficiency of Flag-RIG-I and Cl25-RIG-I to activate the IFN-β promoter after Poly(I:C) transfection. See figure 2 legend for details. (C, D) Lack of co-immunoprecipitation of Cl25-RIG-I with Flag-RIG-I after their co-transfection in Huh7.5 cells and stimulation with Poly(I:C), $^{5'ppp}$ssRNA(62-mer) or $^{5'ppp}$dsRNA(62-mer) (C) or MeV infection (MOI 1) (D) as detected by western blot. (E) Nonsensical co-immunoprecipitation of Cl25-RIG-I with Flag-RIG-I expressed in 293T cells and after transfection of 1 µg or 50 ng of $^{5'ppp}$ds(or ss)RNA(62-mer) or MeV infection (MOI 0.5).
doi:10.1371/journal.pone.0108770.g003

immunoprecipitate decreased with the 62-mer-5′ppp-dsRNA but increased with the 62-mer-5′ppp-ssRNA. Reducing the amounts of transfected RNA and thus the number of RNA molecules accessible for one RIG-I would increase the chance for RIG-I to oligomerize. Since this assessment was only verified for the non-stimulatory ssRNA, we interpret the co-immunoprecipitation of Cl25-RIG-I with Flag-RIG-I as an experimental artefact likely due to over expression of RIG-I in 293T cells. All of these results were repeatedly observed using various experimental conditions, including the use of different lysis buffers.

Search for early induced RIG-I oligomerization *in cellula*

To verify the lack of cognate RNA-induced oligomerization of RIG-I *in cellula*, Huh7.5 cells were co-transfected with Flag-RIG-I and Cl25-RIG-I constructs, stimulated by either Poly(I:C) transfection or Moraten-eGFP infection and harvested 4 hours after stimulation for a co-immunoprecipitation assay. Both Flag-RIG-I and Cl25-RIG-I were expressed in Huh7.5 cells (Figure 4A, inputs). However, upon immunoprecipitation of Flag-RIG-I, Cl25-RIG-I again could not be clearly co-immunoprecipitated. Once more, MeV-N protein could not be detected in the immunoprecipitated fraction (Figure 4A). 293T cells were also used for the investigation of early induced RIG-I oligomerization. As for all experiments, Flag-RIG-I and Cl25-RIG-I were strongly expressed (Figure 4B, inputs), but in these conditions Cl25-RIG-I was evenly found in the Flag eluate independently of cognate RNA stimulation (Figure 4B).

Search for RIG-I oligomerization *in cellula* using a protein complementation assay

We reasoned that the co-immunoprecipitation assay might not be sensitive enough to detect RIG-I oligomerization induced by a cognate RNA. We therefore switched to the *Gaussia* Luciferase-Based Protein Complementation Assay (PCA). PCA has been described to be highly sensitive and have allowed us to detect interactions between monomers in the 0.2–1 µM range [33,45,51]. Cl25-RIG-I and HA-RIG-I coding sequences were fused at either the N- or C-terminus of *Gaussia* glu1 and glu2 split domains. All chimeric proteins were strongly expressed in Huh7.5 cells (Figure 5A). However, we did not detect any luciferase signal that would indicate basal or RNA-induced RIG-I oligomerization *in cellula* with any of the three tested combinations (RIG-I-glu2+glu1-RIG-I; glu2-RIG-I+glu1-RIG-I; RIG-I-glu2+RIG-I-glu1) (Figure 5A). It should be stressed that all glu/RIG-I constructs were able to be activated by a cognate RNA, indicating that grafting glu domains did not prevent RNA recognition by RIG-I. We then tried to force RIG-I dimerization by adding the leucine zipper gcn4 sequence to our constructs [26]. The glu1/2-RIG-I-gcn4 proteins were well expressed in Huh7.5 cells (Figure 5A). The addition of gcn4 sequence induced a modest and significant

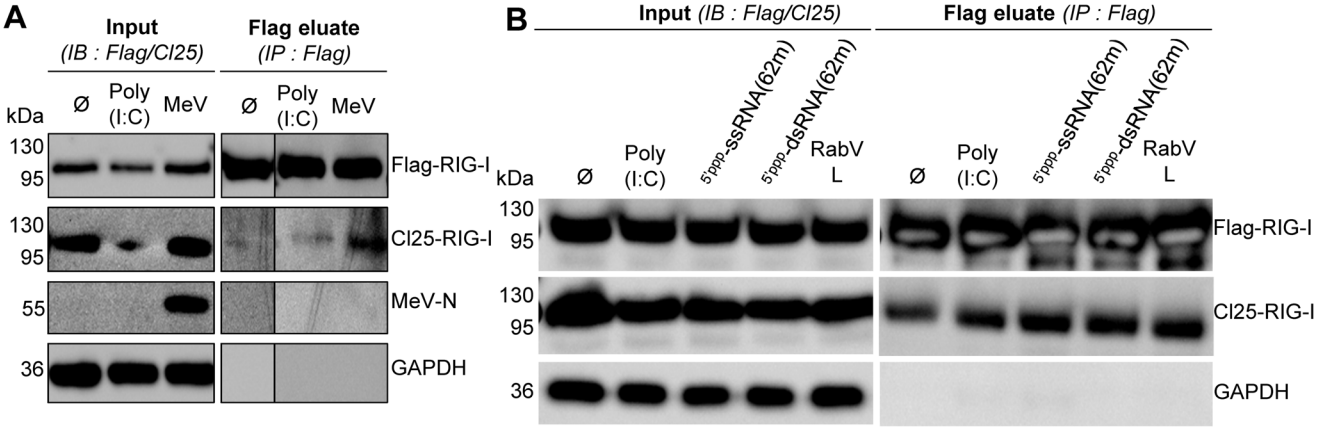

Figure 4. Analysis of RIG-I oligomerization in Huh7.5 (A) and 293T (B) cells determined by co-immunoprecipitation 4 hours after stimulation with Poly(I:C) (A, B), $^{5'ppp}$ssRNA(62-mer), $^{5'ppp}$dsRNA(62-mer) (B) or MeV infection (MOI 1, A, B) of cells expressing Flag-RIG-I and CI25-RIG-I.
doi:10.1371/journal.pone.0108770.g004

luciferase signal, whereas the co-transfection of glu2-gcn4 and glu1-gcn4 induces almost a 3 log higher signal (Figure 5A). Similar results were observed when the luciferase signal was measured only four hours after Poly(I:C) stimulation (Figure S3 in File S1). Moreover, the gcn4 sequence was accessible in the glu1/2-RIG-I-gcn4 chimeric proteins since they readily interacted with free gnc4 construct or gcn4 fused to another protein (Figure S4 in File S1). Correlatively, glu1/2-gcn4 dimerization was easily detected by western blot, while for RIG-I-GCN4 constructs, only a weak dimerization was detected when the glu2-HA-RIG-I-gcn4 protein was expressed alone (Figure 5B).

Discussion

RIG-I oligomerization was proposed to occur during activation by a RNA ligand by two groups in 2007–2008 [14,20]. Since then, the observation of RIG-I oligomerization has progressively become one of the landmarks of RIG-I activation, as many prominent papers in the field tend to report data supporting this idea [7,10,17,18,19,21,49,52,53,54,55]. However, the biochemical support remains rather poor, and the rationale enigmatic.

The RIG-I oligomerization concept originated from *in vitro* analysis by gel filtration of a mixture of pure RIG-I protein and short (from 19 bp to 135 bp) 5′ppp-RNA [10,14,53]. However, a significant shift of the volume of elution observed after chromatography does not necessarily indicate a linear augmentation of mass. Indeed the shape of the molecule can influence its migration properties through the reticulated gel and a conformational change occurs when RIG-I binds an agonist RNA with the tightening of the helicase around the RNA and the release of the CARDs [30,56]. RIG-I oligomerization has also been observed by band shift in Blue Native Gel electrophoresis [20,49]. In addition to some reliability concerns depending on the RNA source used to activate RIG-I [49], a band shift indicates a molecular change and does not necessarily prove oligomerization. The migration properties of a protein can be altered by a small bound RNA that is highly negatively charged and/or by its engagement into a multimolecular complex. In contrast, size-exclusion chromatography on a S200 column coupled to multi-angle laser light scattering analysis of mixtures of pure RIG-I protein with short dsRNA (see Figure S3 in [30] or synthetic *Mononegavirales* leader 5′ppp-RNA (this work) was compatible only with RNA/RIG-I 1:1 monomer complexes. In agreement with our observations, RIG-I and hairpin duplexes of 10, 20 or 30 base pairs with a single 5′ppp end form 1:1 complexes as analysed by analytical ultracentrifugation-sedimentation velocity [8]. Accordingly, crystal structures of RIG-I bound to short RNA (10 mers to 19 mers) shows only monomeric RIG-I:RNA complexes in a 1:1 ratio [30,53,56]. Only when dsRNA contains two 5′ triphosphate ends, could RIG-I:RNA complexes be observed in a 2:1 ratio [8,30]. In these conditions, small angle X-ray scattering indicates that the RIG-I:RNA complex in the 2:1 ratio adopts a very extended conformation [52]. The dimerization of RIG-I CTD reported previously [21,57] may simply reflect the 5′ triphosphorylated bivalency of the dsRNA ligand used. Surprisingly, RIG-I dimerization in the presence of the 62-mer 5′ppp-dsRNA could not be observed *in cellula*. This could be explained by an unbalanced molar ratio of RIG-I protein to 5′ppp-dsRNA in the intracellular milieu, a competition with other 5′ppp-RNA binding proteins and/or the highly dynamic interaction of RIG-I with 5′ppp-dsRNA despite a K_d in the 160 pM range [58].

The incubation of very stable 5′ppp- panhandle RNA with dsRNA of variable length with cellular extracts from RIG-I transfected cells allows the observation of RIG-I oligomerization, at least if the dsRNA exceeds 46 bp in length [54]. According to the proposed model, one molecule of RIG-I would bind the RNA 5′ppp end and enter the RNA using ATP hydrolysis. Several RIG-I molecules would enter an RNA this way and form a RNA mediated oligomer. Contrary to the cooperative association of MDA5 along RNA, RIG-I molecules do not self-oligomerize to form a long filament but multiple proteins can bind to the same RNA, forming a RNA-poly-RIG-I scaffold that falls apart if the long RNA is cleaved by RNAse treatment [18,54,55].

In vivo, RIG-I oligomerization was reported once by pull down assay of Flag- and Myc-tagged RIG-I (see Figure 3 in [20]). However, the lack of clear differences between the data obtained in infected and non-infected cells, questions whether any RNA-induced RIG-I oligomerization had really occurred. In addition, multiple combinations of RIG-I and RIG-I domains and subdomains such as between RIG-I and CARDs, RIG-I and RIG-I-Δ-CARDs, CTD and CARDs, CTD and helicase, CTD and [helicase1+ helicase insertion domain] were also reported. While one cannot exclude that some of the reported interactions could reflect cis-interactions between RIG-I domains bridged or not by viral RNA (such as CTD/Helicase), the other interactions would suggest multiple oligomerization sites within RIG-I.

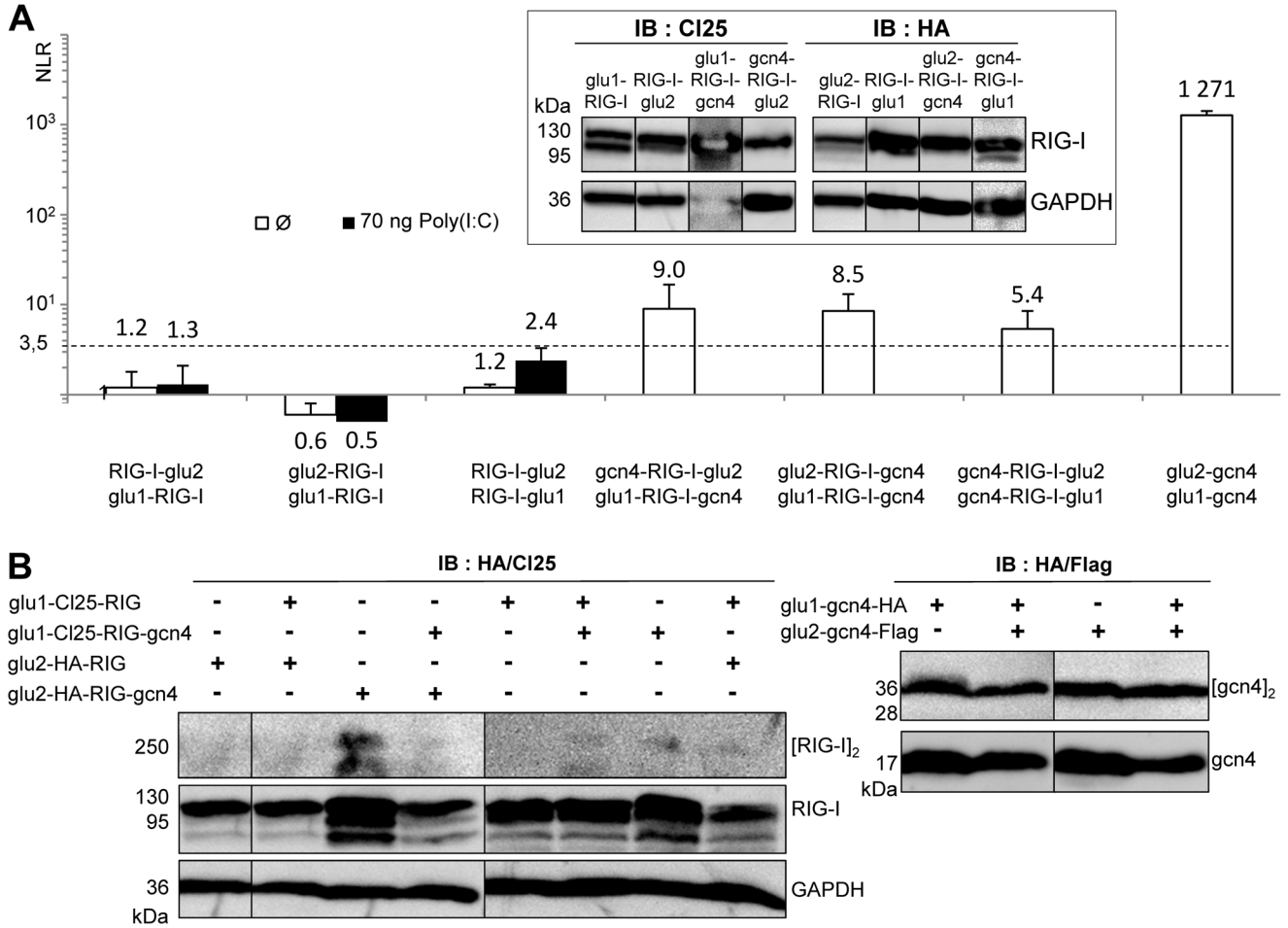

Figure 5. Lack of RNA induced RIG-I oligomerization *in cellula* as detected using PCA. (A) Ability of RIG-I/glu/gcn4 constructs to self-associate in the absence or presence of Poly(I:C) determined by PCA. Luciferase activity was measured 18 hours after transfection or not with Poly(I:C) in 293T cells transfected one day before with RIG-I/glu1/2/gcn4 constructs. (A, inset) Expression of chimeric RIG-I/glu1/2 constructs tagged with CI25 or HA peptides in Huh7.5 cells two days after transfection as detected by western blot (note that the third sample (Glu1-RIG-I-GCN4 was overloaded, hence the overexposure of this protein and GAPDH). (B) Ability of RIG-I/glu/gcn4 chimeric proteins (left panel) and glu-gcn4 protein (right panel) for self-binding determined by western blot 24 hours post-transfection of 293T cells with glu1 or glu2 constructs alone or in combination. Lysates were separated without prior heat denaturation on SDS-PAGE before western blot analysis.
doi:10.1371/journal.pone.0108770.g005

However, none of them are supported by available RIG-I crystal structures. In contrast, in our work, we did not observe self-assembly of RIG-I upon recognition of synthetic or viral RNA by co-immunoprecipitation assay or using the more sensitive PCA assay. Furthermore, RIG-I dimerization hardly occurred even after being grafted with the gcn4 dimerization signal.

We strongly favour that a monomeric RIG-I-RNA complex is the minimal functional signal transduction unit in full agreement with biochemically defined monomeric RIG-I-RNA complexes that are able to activate the IFN response [8,54]. Thus, so far there is no convincing evidence that, upon RNA recognition, RIG-I could (or should) self-oligomerize (i.e. via direct protein-protein interaction), and the model of RIG-I oligomerization for enabling signal transduction is inconsistent with all cell biological, biochemical and structural biological studies that have endeavoured to quantitatively assess the stoichiometry of RIG-I in its activated state. Rather, a single dsRNA can bind several RIG-I molecules and this can occur or not during viral infection [49] (and this work). Further down the signalling cascade, tandem CARDs of RIG-I associate with free K63 polyubiquitin in a helical tetramer complex [59] that becomes engaged in a complex interaction with membrane anchored MAVS. This scaffold would associate multiple RNA-RIG-I signal units to several MAVS molecules [12,13,53,60,61,62,63,64]. Interestingly, this polyubiquitin-dependent scaffolding appears to be dispensable when several RIG-I molecules are associated with one long RNA [55] in agreement with RIG-I CARD tandem forming complexes with MAVS CARD [65].

Supporting Information

File S1 Contains Figure S1, Efficient infection of Huh7.5 cells by Moraten-gfp MeV strain, at MOI 1. Vero cells and Huh7.5 cells were harvested 30 hours after infection and analyzed by flow cytometry for GFP expression with mean florescence intensity (left) and % of GFP expressing cells (right). Figure S2, The anti-Flag immunoprecipitation procedure can detect complex formation between MeV N and FLAG-P proteins. Vero cells were infected with two measles viruses expressing a wt P protein or a Flag-tagged P protein at MOI 0.1. The cell extracts, collected 20 h after infection, were immunoprecipitated with Flag antibody coupled to beads. Proteins eluted with Flag peptide were analyzed by western

blot using anti-P 49.21 and anti-N Cl25 monoclonal antibodies. Note the exclusive pull-down of N from cells infected with the Flag-P virus. Figure S3, Ability of RIG-I/glu/gcn4 constructs for self-binding in absence or presence of Poly(I:C) determined by PCA. Luciferase activity was measured 4 hours after transfection or not with Poly(I:C) in 293T cells expressing RIG-I/glu1/2/gcn4 constructs. Figure S4, Accessibility of gcn4 sequence in RIG-I/glu/gcn4 constructs for determination of RIG-I oligomerization by PCA. Luciferase activity was measured 24 hours after transfection of RIG-I/glu1/2/gcn4, gcn4/glu1/2 and MeV Ntail/XD/glu1/2/gcn4 constructs in 293T cells.
(PDF)

Acknowledgments

The authors thank Y. Jacob, D. Garcin, T. Fujita, P. Pothier, C. Rice, T. Imaizumi and R. Cattaneo for providing us with useful reagents, C. Lazert, L. Wouters and M. Ferren for plasmid construction and P Lawrence for English proofreading and copiediting. We thank T. Crepin for the clone of influenza panhandle RNA and P. Holenya for help with RNA preparations, the beamline staff of ID14-2 at ESRF, Grenoble, France, the flow cytometry (T. Andrieu, S. Dussurgey) and qPCR (B. Blanquier) facilities of the SFR Biosciences Gerland-Lyon Sud (UMS344/US8).

Author Contributions

Conceived and designed the experiments: JL EK LMB SC DG. Performed the experiments: JL LMB EK JB. Analyzed the data: JL LMB EK SC DG. Contributed reagents/materials/analysis tools: LMB EK JB. Wrote the paper: JL LMB DG EK.

References

1. Ranjan P, Bowzard JB, Schwerzmann JW, Jeisy-Scott V, Fujita T, et al. (2009) Cytoplasmic nucleic acid sensors in antiviral immunity. Trends in molecular medicine 15: 359–368.
2. Yoneyama M, Fujita T (2009) RNA recognition and signal transduction by RIG-I-like receptors. Immunological Reviews 227: 54–65.
3. Onoguchi K, Yoneyama M, Fujita T (2011) Retinoic acid-inducible gene-I-like receptors. Journal of interferon & cytokine research: the official journal of the International Society for Interferon and Cytokine Research 31: 27–31.
4. Wilkins C, Gale M Jr (2010) Recognition of viruses by cytoplasmic sensors. Current opinion in Immunology 22: 41–47.
5. Yoneyama M, Fujita T (2007) RIG-I family RNA helicases: cytoplasmic sensor for antiviral innate immunity. Cytokine Growth Factor Reviews 18: 545–551.
6. Yoneyama M, Fujita T (2010) Recognition of viral nucleic acids in innate immunity. Reviews in medical virology 20: 4–22.
7. Binder M, Eberle F, Seitz S, Mucke N, Huber CM, et al. (2011) Molecular mechanism of signal perception and integration by the innate immune sensor retinoic acid-inducible gene-I (RIG-I). The Journal of biological chemistry 286: 27278–27287.
8. Kohlway A, Luo D, Rawling DC, Ding SC, Pyle AM (2013) Defining the functional determinants for RNA surveillance by RIG-I. EMBO reports 14: 772–779.
9. Schlee M, Roth A, Hornung V, Hagmann CA, Wimmenauer V, et al. (2009) Recognition of 5′ triphosphate by RIG-I helicase requires short blunt double-stranded RNA as contained in panhandle of negative-strand virus. Immunity 31: 25–34.
10. Schmidt A, Schwerd T, Hamm W, Hellmuth JC, Cui S, et al. (2009) 5′-triphosphate RNA requires base-paired structures to activate antiviral signaling via RIG-I. Proceedings of the National Academy of Sciences of the United States of America 106: 12067–12072.
11. Dixit E, Kagan JC (2013) Intracellular pathogen detection by RIG-I-like receptors. Advances in immunology 117: 99–125.
12. Gack MU, Shin YC, Joo CH, Urano T, Liang C, et al. (2007) TRIM25 RING-finger E3 ubiquitin ligase is essential for RIG-I-mediated antiviral activity. Nature 446: 916–920.
13. Zeng W, Sun L, Jiang X, Chen X, Hou F, et al. (2010) Reconstitution of the RIG-I pathway reveals a signaling role of unanchored polyubiquitin chains in innate immunity. Cell 141: 315–330.
14. Cui S, Eisenacher K, Kirchhofer A, Brzozka K, Lammens A, et al. (2008) The C-terminal regulatory domain is the RNA 5′-triphosphate sensor of RIG-I. Molecular Cell 29: 169–179.
15. Jiang X, Kinch LN, Brautigam CA, Chen X, Du F, et al. (2012) Ubiquitin-induced oligomerization of the RNA sensors RIG-I and MDA5 activates antiviral innate immune response. Immunity 36: 959–973.
16. Li X, Lu C, Stewart M, Xu H, Strong RK, et al. (2009) Structural basis of double-stranded RNA recognition by the RIG-I like receptor MDA5. Archives in Biochemistry and Biophysics 488: 23–33.
17. Lu C, Xu H, Ranjith-Kumar CT, Brooks MT, Hou TY, et al. (2010) The structural basis of 5′ triphosphate double-stranded RNA recognition by RIG-I C-terminal domain. Structure 18: 1032–1043.
18. Peisley A, Lin C, Wu B, Orme-Johnson M, Liu M, et al. (2011) Cooperative assembly and dynamic disassembly of MDA5 filaments for viral dsRNA recognition. Proceedings of the National Academy of Sciences of the United States of America 108: 21010–21015.
19. Ranjith-Kumar CT, Murali A, Dong W, Srisathiyanarayanan D, Vaughan R, et al. (2009) Agonist and antagonist recognition by RIG-I, a cytoplasmic innate immunity receptor. The Journal of biological chemistry 284: 1155–1165.
20. Saito T, Hirai R, Loo YM, Owen D, Johnson CL, et al. (2007) Regulation of innate antiviral defenses through a shared repressor domain in RIG-I and LGP2. Proceedings of the National Academy of Sciences of the United States of America 104: 582–587.
21. Wang Y, Ludwig J, Schuberth C, Goldeck M, Schlee M, et al. (2010) Structural and functional insights into 5′-ppp RNA pattern recognition by the innate immune receptor RIG-I. Nature structural & molecular biology 17: 781–787.
22. Blight KJ, McKeating JA, Rice CM (2002) Highly permissive cell lines for subgenomic and genomic hepatitis C virus RNA replication. Journal of virology 76: 13001–13014.
23. Yasumura Y, Kawakita M (1963) The research for the SV40 by means of tissue culture technique. Nippon Rinsho 21: 1201–1219.
24. Graham FL, Smiley J, Russell WC, Nairn R (1977) Characteristics of a human cell line transformed by DNA from human adenovirus type 5. The Journal of general virology 36: 59–74.
25. Radecke F, Spielhofer P, Schneider H, Kaelin K, Huber M, et al. (1995) Rescue of measles viruses from cloned DNA. EMBO Journal 14: 5773–5784.
26. O'Shea EK, Klemm JD, Kim PS, Alber T (1991) X-ray structure of the GCN4 leucine zipper, a two-stranded, parallel coiled coil. Science 254: 539–544.
27. Giraudon P, Jacquier MF, Wild TF (1988) Antigenic analysis of African measles virus field isolates: identification and localisation of one conserved and two variable epitope sites on the NP protein. Virus Research 10: 137–152.
28. Chen M, Cortay JC, Logan IR, Sapountzi V, Robson CN, et al. (2005) Inhibition of ubiquitination and stabilization of human ubiquitin E3 ligase PIRH2 by measles virus phosphoprotein. Journal of virology 79: 11824–11836.
29. Imaizumi T, Aratani S, Nakajima T, Carlson M, Matsumiya T, et al. (2002) Retinoic acid-inducible gene-I is induced in endothelial cells by LPS and regulates expression of COX-2. Biochemical and biophysical research communications 292: 274–279.
30. Kowalinski E, Lunardi T, McCarthy AA, Louber J, Brunel J, et al. (2011) Structural basis for the activation of innate immune pattern-recognition receptor RIG-I by viral RNA. Cell 147: 423–435.
31. Marq JB, Hausmann S, Veillard N, Kolakofsky D, Garcin D (2011) Short double-stranded RNAs with an overhanging 5′ ppp-nucleotide, as found in arenavirus genomes, act as RIG-I decoys. The Journal of biological chemistry 286: 6108–6116.
32. Zimm BH (1948) The dependence of the scattering of light on angle and concentration in linear polymer solutions. The Journal of physical and colloid chemistry 52: 260–267.
33. Cassonnet P, Rolloy C, Neveu G, Vidalain PO, Chantier T, et al. (2011) Benchmarking a luciferase complementation assay for detecting protein complexes. Nature methods 8: 990–992.
34. Chen C, Ridzon DA, Broomer AJ, Zhou Z, Lee DH, et al. (2005) Real-time quantification of microRNAs by stem-loop RT-PCR. Nucleic acids research 33: e179.
35. Eguchi H, Nagano H, Yamamoto H, Miyamoto A, Kondo M, et al. (2000) Augmentation of antitumor activity of 5-fluorouracil by interferon alpha is associated with up-regulation of p27Kip1 in human hepatocellular carcinoma cells. Clinical cancer research: an official journal of the American Association for Cancer Research 6: 2881–2890.
36. Keskinen P, Nyqvist M, Sareneva T, Pirhonen J, Melen K, et al. (1999) Impaired antiviral response in human hepatoma cells. Virology 263: 364–375.
37. Li K, Chen Z, Kato N, Gale M Jr, Lemon SM (2005) Distinct poly(I-C) and virus-activated signaling pathways leading to interferon-beta production in hepatocytes. The Journal of biological chemistry 280: 16739–16747.
38. Sumpter R Jr, Loo YM, Foy E, Li K, Yoneyama M, et al. (2005) Regulating intracellular antiviral defense and permissiveness to hepatitis C virus RNA replication through a cellular RNA helicase, RIG-I. Journal of virology 79: 2689–2699.
39. Marq JB, Kolakofsky D, Garcin D (2010) Unpaired 5′ ppp-nucleotides, as found in arenavirus double-stranded RNA panhandles, are not recognized by RIG-I. The Journal of biological chemistry 285: 18208–18216.
40. Runge S, Sparrer KM, Lassig C, Hembach K, Baum A, et al. (2014) In Vivo Ligands of MDA5 and RIG-I in Measles Virus-Infected Cells. PLoS Pathogens 10: e1004081.

41. Bamming D, Horvath CM (2009) Regulation of signal transduction by enzymatically inactive antiviral RNA helicase proteins MDA5, RIG-I, and LGP2. The Journal of biological chemistry 284: 9700–9712.
42. Plumet S, Herschke F, Bourhis JM, Valentin H, Longhi S, et al. (2007) Cytosolic 5′-triphosphate ended viral leader transcript of measles virus as activator of the RIG I-mediated interferon response. PLoS One 2: e279.
43. Takahasi K, Kumeta H, Tsuduki N, Narita R, Shigemoto T, et al. (2009) Solution structures of cytosolic RNA sensor MDA5 and LGP2 C-terminal domains: identification of the RNA recognition loop in RIG-I-like receptors. The Journal of biological chemistry 284: 17465–17474.
44. Blocquel D, Habchi J, Costanzo S, Doizy A, Oglesbee M, et al. (2012) Interaction between the C-terminal domains of measles virus nucleoprotein and phosphoprotein: a tight complex implying one binding site. Protein science: a - publication of the Protein Society 21: 1577–1585.
45. Brunel J, Chopy D, Dosnon M, Bloyet LM, Devaux P, et al. (2014) Sequence of events in measles virus replication: role of phosphoprotein-nucleocapsid interactions. Journal of virology 88: 10851–10863.
46. Gely S, Lowry DF, Bernard C, Jensen MR, Blackledge M, et al. (2010) Solution structure of the C-terminal X domain of the measles virus phosphoprotein and interaction with the intrinsically disordered C-terminal domain of the nucleoprotein. Journal of molecular recognition: JMR 23: 435–447.
47. Longhi S (2009) Nucleocapsid structure and function. Current topics in microbiology and immunology 329: 103–128.
48. Shu Y, Habchi J, Costanzo S, Padilla A, Brunel J, et al. (2012) Plasticity in structural and functional interactions between the phosphoprotein and nucleoprotein of measles virus. The Journal of biological chemistry 287: 11951–11967.
49. Weber M, Gawanbacht A, Habjan M, Rang A, Borner C, et al. (2013) Incoming RNA virus nucleocapsids containing a 5′-triphosphorylated genome activate RIG-I and antiviral signaling. Cell host & microbe 13: 336–346.
50. Gerlier D, Lyles DS (2011) Interplay between innate immunity and negative-strand RNA viruses: towards a rational model. Microbiology and molecular biology reviews: MMBR 75: 468–490.
51. Remy I, Michnick SW (2006) A highly sensitive protein-protein interaction assay based on Gaussia luciferase. Nature methods 3: 977–979.
52. Beckham SA, Brouwer J, Roth A, Wang D, Sadler AJ, et al. (2013) Conformational rearrangements of RIG-I receptor on formation of a multi-protein: dsRNA assembly. Nucleic acids research 41: 3436–3445.
53. Jiang F, Ramanathan A, Miller MT, Tang GQ, Gale M, et al. (2011) Structural basis of RNA recognition and activation by innate immune receptor RIG-I. Nature 479: 423–427.
54. Patel JR, Jain A, Chou YY, Baum A, Ha T, et al. (2013) ATPase-driven oligomerization of RIG-I on RNA allows optimal activation of type-I interferon. EMBO reports 14: 780–787.
55. Peisley A, Wu B, Yao H, Walz T, Hur S (2013) RIG-I forms signaling-competent filaments in an ATP-dependent, ubiquitin-independent manner. Molecular cell 51: 573–583.
56. Luo D, Ding SC, Vela A, Kohlway A, Lindenbach BD, et al. (2011) Structural Insights into RNA Recognition by RIG-I. Cell 147: 409–422.
57. Li X, Ranjith-Kumar CT, Brooks MT, Dharmaiah S, Herr AB, et al. (2009) The RIG-I-like receptor LGP2 recognizes the termini of double-stranded RNA. The Journal of biological chemistry 284: 13881–13891.
58. Vela A, Fedorova O, Ding SC, Pyle AM (2012) The thermodynamic basis for viral RNA detection by the RIG-I innate immune sensor. The Journal of biological chemistry 287: 42564–42573.
59. Peisley A, Wu B, Xu H, Chen ZJ, Hur S (2014) Structural basis for ubiquitin-mediated antiviral signal activation by RIG-I. Nature 509: 110–114.
60. Kolakofsky D, Kowalinski E, Cusack S (2012) A structure-based model of RIG-I activation. RNA 18: 2118–2127.
61. Hou F, Sun L, Zheng H, Skaug B, Jiang QX, et al. (2011) MAVS forms functional prion-like aggregates to activate and propagate antiviral innate immune response. Cell 146: 448–461.
62. Moresco EM, Beutler B (2010) LGP2: positive about viral sensing. Proceedings of the National Academy of Sciences of the United States of America 107: 1261–1262.
63. Fitzgerald ME, Rawling DC, Vela A, Pyle AM (2014) An evolving arsenal: viral RNA detection by RIG-I-like receptors. Current opinion in microbiology 20C: 76–81.
64. Rawling DC, Pyle AM (2014) Parts, assembly and operation of the RIG-I family of motors. Current opinion in structural biology 25: 25–33.
65. Wu B, Peisley A, Tetrault D, Li Z, Egelman EH, et al. (2014) Molecular Imprinting as a Signal-Activation Mechanism of the Viral RNA Sensor RIG-I. Molecular cell 55: 511–523.

LETTER

doi:10.1038/nature13596

A long noncoding RNA protects the heart from pathological hypertrophy

Pei Han[1,2], Wei Li[1,2]*, Chiou-Hong Lin[2]*, Jin Yang[1], Ching Shang[2], Sylvia T. Nurnberg[2], Kevin Kai Jin[2], Weihong Xu[3], Chieh-Yu Lin[2], Chien-Jung Lin[2], Yiqin Xiong[2], Huan-Chieh Chien[2], Bin Zhou[4], Euan Ashley[2], Daniel Bernstein[5], Peng-Sheng Chen[1], Huei-Sheng Vincent Chen[6], Thomas Quertermous[2] & Ching-Pin Chang[1,7,8]

The role of long noncoding RNA (lncRNA) in adult hearts is unknown; also unclear is how lncRNA modulates nucleosome remodelling. An estimated 70% of mouse genes undergo antisense transcription[1], including myosin heavy chain 7 (*Myh7*), which encodes molecular motor proteins for heart contraction[2]. Here we identify a cluster of lncRNA transcripts from *Myh7* loci and demonstrate a new lncRNA–chromatin mechanism for heart failure. In mice, these transcripts, which we named myosin heavy-chain-associated RNA transcripts (*Myheart*, or *Mhrt*), are cardiac-specific and abundant in adult hearts. Pathological stress activates the Brg1–Hdac–Parp chromatin repressor complex[3] to inhibit *Mhrt* transcription in the heart. Such stress-induced *Mhrt* repression is essential for cardiomyopathy to develop: restoring *Mhrt* to the pre-stress level protects the heart from hypertrophy and failure. *Mhrt* antagonizes the function of Brg1, a chromatin-remodelling factor that is activated by stress to trigger aberrant gene expression and cardiac myopathy[3]. *Mhrt* prevents Brg1 from recognizing its genomic DNA targets, thus inhibiting chromatin targeting and gene regulation by Brg1. It does so by binding to the helicase domain of Brg1, a domain that is crucial for tethering Brg1 to chromatinized DNA targets. Brg1 helicase has dual nucleic-acid-binding specificities: it is capable of binding lncRNA (*Mhrt*) and chromatinized—but not naked—DNA. This dual-binding feature of helicase enables a competitive inhibition mechanism by which *Mhrt* sequesters Brg1 from its genomic DNA targets to prevent chromatin remodelling. A *Mhrt*–Brg1 feedback circuit is thus crucial for heart function. Human *MHRT* also originates from *MYH7* loci and is repressed in various types of myopathic hearts, suggesting a conserved lncRNA mechanism in human cardiomyopathy. Our studies identify a cardioprotective lncRNA, define a new targeting mechanism for ATP-dependent chromatin-remodelling factors, and establish a new paradigm for lncRNA–chromatin interaction.

By 5′ and 3′ rapid amplification of complementary DNA ends, we discovered an alternative splicing of *Myh7* antisense transcription into a cluster of RNAs of 709 to 1,147 nucleotides (*Mhrt* RNAs), containing partial sequences of *Myh7* introns and exons (Fig. 1a and Supplementary Note). *Mhrt* RNAs were cardiac-specific (Fig. 1b), present at low levels in fetal hearts, with increasing abundance as the hearts matured and *Myh6*/*Myh7* ratio increased (Fig. 1c). RNA *in situ* analysis showed that *Mhrt* RNAs resided in the myocardium but not endocardium or epicardium (Fig. 1d and Extended Data Fig. 1a). Quantification of nuclear/cytoplasmic RNA in heart extracts revealed that *Mhrt* transcripts were primarily nuclear RNAs (Fig. 1e). Coding substitution frequencies[4,5] of *Mhrt* RNAs predicted a negative/low protein-coding potential, *in vitro* translation of *Mhrt* RNAs yielded no proteins, and ribosome profiling[6] revealed no/minimal ribosomes on *Mhrt* (Fig. 1f, Extended Data Fig. 1b–f and Supplementary Note). Consequently, *Mhrt* RNAs are non-coding RNAs in cardiomyocyte nuclei.

Mhrt RNAs were downregulated by 46–68% in hearts pressure-overloaded by transaortic constriction (TAC)[3], beginning by 2 days and lasting for ≥42 days after TAC (Fig. 2a). Such *Mhrt* reduction coincided with the TAC-induced *Myh6* to *Myh7* isoform switch characteristic of cardiomyopathy[7–9] (Extended Data Fig. 2a). To define *Mhrt* function, we focused on *Mhrt779,* the most abundant *Mhrt* species, with 779 nucleotides (Fig. 2b, c and Extended Data Fig. 2b–e). We generated a transgenic mouse line to restore *Mhrt779* level in stressed hearts. This transgenic line, driven by tetracycline response element (*Tre-Mhrt779*), was crossed to a cardiac-specific driver line (*Tnnt2-rtTA*)[3] that employs troponin promoter (*Tnnt2*) to direct expression of reverse tetracycline-dependent transactivator (rtTA). The resulting *Tnnt2-rtTA*;*Tre-Mhrt779* line (abbreviated as *Tg779*) enabled the use of doxycycline to induce *Mhrt779* expression in cardiomyocytes. Within 7–14 days of doxycycline treatment, *Mhrt779* increased by ~1.5-fold in left ventricles of *Tg779* mice; this offset *Mhrt779* suppression in TAC-stressed hearts to maintain *Mhrt779* at the pre-stress level (Fig. 2d). Six weeks after TAC, doxycycline-treated control mice (*Tre-Mhrt779*, *Tnnt2-rtTA* or wild type) developed severe cardiac hypertrophy and fibrosis with left ventricular dilatation and reduced fractional shortening. Conversely, doxycycline-treated *Tg779* hearts—with *Mhrt779* maintained at the pre-stress level—developed much less pathology, with a 45.7% reduction in the ventricle/body-weight ratio (Fig. 2e) and a 61.3% reduction in cardiomyocyte size (Fig. 2f and Extended Data Fig. 3a), minimal/absent cardiac fibrosis (Fig. 2g), a 45.5% improvement of fractional shortening (Fig. 2h and Extended Data Fig. 3b), normalized left ventricular size (Fig. 2i), and reduced pathological changes of *Anf* (also known as *Nppa*), *Bnp* (also known as *Nppb*), *Serca2* (also known as *Atp2a2*), *Tgfb1* and *Opn* (also known as *Spp1*) expression[10–13] (Extended Data Figs 3c and 6e). To further test the cardioprotective effects of *Mhrt*, we induced *Mhrt779* after 1–2 weeks of TAC when hypertrophy had begun. This approach reduced hypertrophy by 23% and improved fractional shortening by 33% in 8 weeks after TAC (Extended Data Fig. 3d–f). The efficacy of late *Mhrt779* introduction suggests that a sustained repression of *Mhrt* in stressed hearts is essential for continued decline of cardiac function.

To study *Mhrt* regulation, we examined the 5′ upstream region of the *Mhrt* genomic site (−2329 to +143) (Extended Data Fig. 4a) for signatures of a lncRNA promoter: RNA polymerase II (Pol II), histone H3 trimethylated lysine 4 (H3K4me3) and histone H3 trimethylated lysine 36 (H3K36me3)[4,14,15]. By chromatin immunoprecipitation (ChIP) of left ventricles, we found that this putative promoter contained four evolutionarily conserved elements (a1 to a4)[3] that were enriched with Pol II

[1]Krannert Institute of Cardiology and Division of Cardiology, Department of Medicine, Indiana University School of Medicine, Indianapolis, Indiana 46202, USA. [2]Division of Cardiovascular Medicine, Cardiovascular Institute, Stanford University School of Medicine, Stanford, California 94305, USA. [3]Stanford Genome Technology Center, Stanford University School of Medicine, Stanford, California 94305, USA. [4]Department of Genetics, Pediatrics, and Medicine (Cardiology), Albert Einstein College of Medicine of Yeshiva University, 1301 Morris Park Avenue, Price Center 420, Bronx, New York 10461, USA. [5]Department of Pediatrics, Stanford University School of Medicine, Stanford, California 94305, USA. [6]Del E. Webb Neuroscience, Aging & Stem Cell Research Center, Sanford/Burnham Medical Research Institute, La Jolla, California 92037, USA. [7]Department of Biochemistry and Molecular Biology, Indiana University School of Medicine, Indianapolis, Indiana 46202, USA. [8]Department of Medical and Molecular Genetics, Indiana University School of Medicine, Indianapolis, Indiana 46202, USA.
*These authors contributed equally to this work.

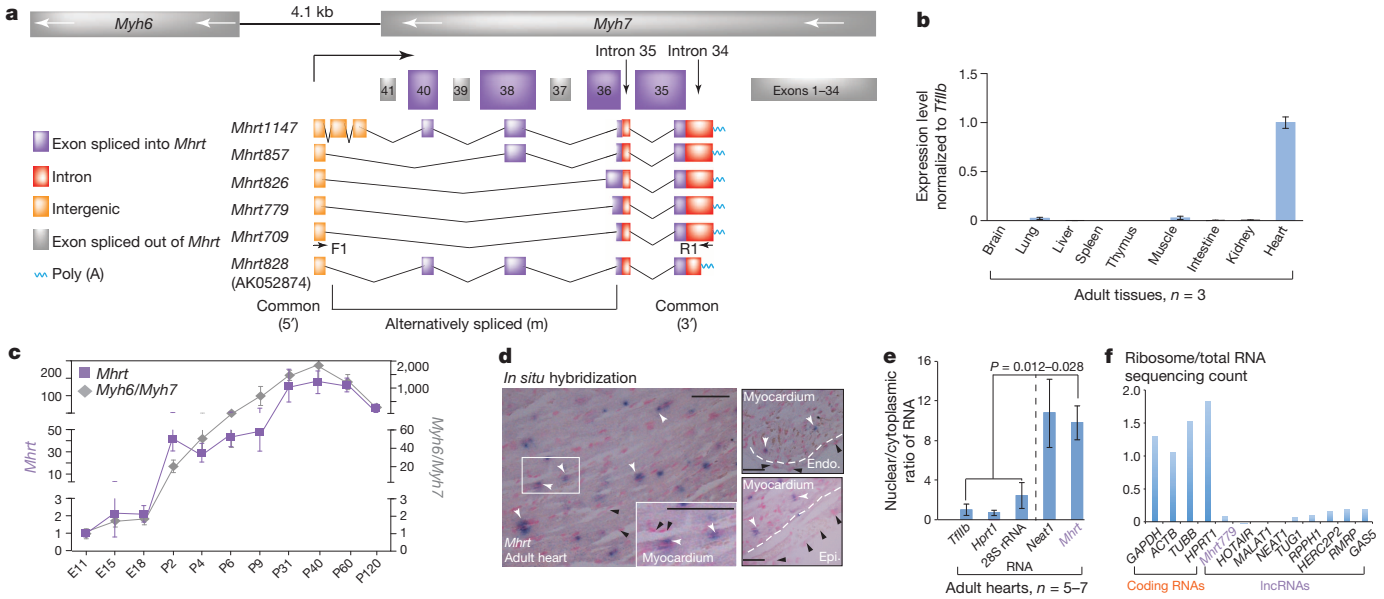

Figure 1 | Profile of the noncoding RNA *Mhrt*. **a**, Schematic illustration of *Mhrt* RNAs originating from the intergenic region between *Myh6* and *Myh7* and transcribed into *Myh7*. *Myh7* exons and introns are indicated. m, mid region of the RNAs. F1 and R1, targeting the 5′ and 3′ *Mhrt* common sequences, are the primers used for subsequent polymerase chain reaction (PCR). **b**, Quantitative PCR with reverse transcription (RT–qPCR) of *Mhrt* RNAs using primers targeting common regions of *Mhrt* RNAs in tissues from 2-month-old mice. **c**, RT–qPCR of *Mhrt*, *Myh6* and *Myh7* in mouse hearts at different ages. *Mhrt* and *Myh6*/*Myh7* ratio of embryonic day (E)11 hearts are set as 1. P, postnatal day. **d**, RNA *in situ* analysis of *Mhrt* (blue) in adult hearts. The RNA probe targets all *Mhrt* species. Red: nuclear fast red. White arrowheads indicate myocardial nuclei. Black arrowheads indicate nuclei of endothelial, endocardial or epicardial cells. Dashed lines demarcate the myocardium from endocardium (Endo.) or from epicardium (Epi.). Scale bars = 50 μm. **e**, RT–qPCR of nuclear/cytoplasmic RNA in adult hearts. *Tfllb* (also known as *Gtf2b*), *Hprt1* and 28S rRNA are primarily cytoplasmic RNAs; *Neat1*, nuclear lncRNA. *Tfllb* ratio is set as 1. **f**, Ribosome profiling: ribosome density on coding RNAs and lncRNAs. *P* values: Student's *t*-test. Error bars show standard error of the mean (s.e.m.).

(a1 to a4), H3K4me3 (a1 and a4) and H3K36me3 (refs 14, 16–18) (a1 and a3/a4) (Extended Data Fig. 4a–d). Conversely, no Pol II, H3K4me3 or H3K36me3 enrichment was found in control *Shh* and *Vegfa* promoters or in thymus and lungs that did not express *Mhrt* RNAs (Extended Data Fig. 4b–d). These results reveal an active, cardiac-specific lncRNA promoter controlling *Mhrt* expression.

We then asked how *Mhrt* was repressed in stressed hearts. We postulated that cardiac stress activated Brg1, leading it to occupy the a1–a4 promoter and to repress *Myh6* (ref. 3) and *Mhrt* in opposite transcription directions (Extended Data Fig. 4a). Indeed, *Mhrt* repression required Brg1: TAC suppressed *Mhrt* RNAs in control but not *Brg1*-null hearts (*Tnnt2-rtTA;Tre-Cre;Brg1*$^{fl/fl}$)[3] (Extended Data Fig. 4e). To test Brg1 activity on the *Mhrt* promoter, we cloned the a1–a4 promoter in the *Mhrt* transcription direction (−2329 to +143) into an episomal luciferase reporter, pREP4, that allows promoter chromatinization[19]. Brg1 was then transfected into Brg1-deficient SW13 cells[20] to reconstitute the Brg1/BAF complex for reporter assays. Brg1 transfection caused a ~50% reduction of *Mhrt* promoter activity ($P < 0.0001$), and such *Mhrt* repression was virtually abolished by Hdac inhibition with trichostatin-A or Parp inhibition

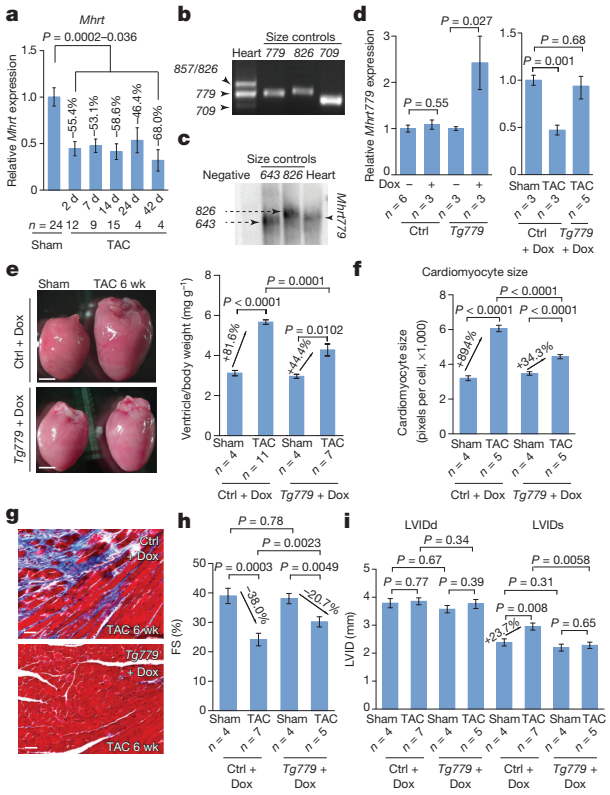

Figure 2 | *Mhrt* inhibits cardiac hypertrophy and failure. **a**, Quantification of cardiac *Mhrt* RNAs 2–42 days (d) after TAC operation. **b**, RT–PCR of *Mhrt* RNAs in adult heart ventricles. Primers (F1 and R1; Fig. 1a) target *Mhrt* common regions. Size controls *779*, *826* and *709* are PCR products of recombinant *Mhrt779*, *Mhrt826* and *Mhrt709*, respectively. **c**, Northern blot of *Mhrt* RNAs in adult heart ventricles. The probe targets common regions of *Mhrt* RNAs. Negative: control RNA from 293T cells. Size control *826* is recombinant *Mhrt826*; *643* (not a distinct *Mhrt* species) contains the 5′ common region of *Mhrt*. **d**, Quantification of *Mhrt779* in control or *Tg779* mice with or without doxycycline (Dox) or TAC operation. *Mhrt779*-specific PCR primers were used. Ctrl, control mice. **e**, Ventricle/body-weight ratio of hearts 6 weeks (wk) after TAC. Scale bars = 1 mm. **f**, Quantification of cardiomyocyte size in control and *Tg779* mice 6 weeks after TAC by wheat-germ agglutinin staining. **g**, Trichrome staining in control and *Tg779* hearts 6 weeks after TAC. Red indicates cardiomyocytes; blue indicates fibrosis. Scale bars = 20 μm. **h**, **i**, Echocardiographic measurement of left ventricular fractional shortening (FS; **h**) and internal dimensions at end-diastole (LVIDd) and end-systole (LVIDs) (**i**) 6 weeks after TAC. *P* values: Student's *t*-test. Error bars show s.e.m.

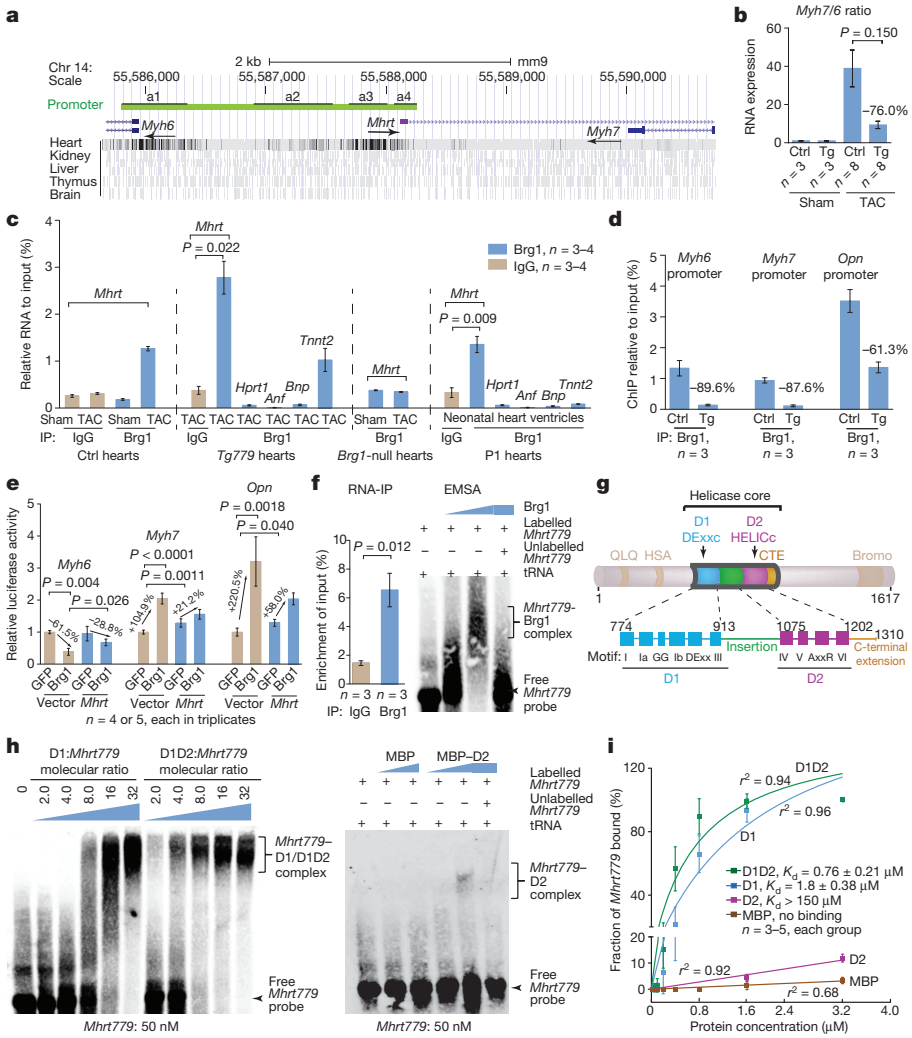

Figure 3 | *Mhrt* complexes with Brg1 through the helicase domain. **a**, DNaseI digital footprinting of *Myh6/Mhrt* promoter loci from ENCODE. *Myh6* and *Mhrt* are transcribed in opposite directions as indicated by arrows. Bars represent DNA fragments protected from DNaseI digestion. Black boxes (a1–a4) refer to promoter regions with high sequence homology (Extended Data Fig. 4a). **b**, Quantification of *Myh7/Myh6* ratio in control (Ctrl) and *Tg779* (Tg) hearts 2 weeks after TAC. **c**, RNA-immunoprecipitation (IP) of *Mhrt*–Brg1 in ventricles from control hearts (Ctrl) with sham/TAC operation; *Tg779* hearts after TAC; *Brg1*-null (*Tnnt2-rtTA;Tre-Cre;Brg1*$^{fl/fl}$) hearts after TAC; and P1 hearts. **d**, ChIP analysis of Brg1 in control (Ctrl) and *Tg779* hearts 2 weeks after TAC. **e**, Luciferase reporter assay of *Myh6* and *Myh7* promoters in neonatal rat cardiomyocytes. *Mhrt*, pAdd2-*Mhrt779*; Vector, pAdd2 empty vector. **f**, RNA-IP and EMSA of recombinant Brg1 proteins and *in vitro* transcribed *Mhrt779*. Biotin-labelled *Mhrt779*: 50 nM; unlabelled *Mhrt779*: 500 nM. **g**, Schematics of mouse Brg1 protein. The helicase core includes the DExx-c and HELIC-c domain. **h**, EMSA of *Mhrt779* and Brg1 helicase. **i**, Binding affinity of *Mhrt779* for MBP-tagged D1D2 determined by EMSA. Data are from multiple independent measurements. Nonlinear regression curves were generated by GraphPad Prism. *P* values: Student's *t*-test. Error bars show s.e.m.

with PJ-34 (ref. 21) (Extended Data Fig. 4f), indicating a cooperative repressor function between Brg1, Hdac and Parp. ChIP verified that the *Mhrt* promoter (a1–a4) was occupied by Brg1, Hdac2/9 and Parp1 in stressed hearts[3] and in the pREP4 reporter episome (Extended Data Fig. 4g). These findings indicate that *Mhrt* is repressed by the stress-induced Brg1–Hdac–Parp complex[3] through the a1–a4 promoter.

Because *Myh6* and *Mhrt* were both regulated by the a1–a4 promoter, we hypothesized that a1–a4 contained two elements to regulate *Myh6* and *Mhrt*—with the a1 element controlling *Myh6* and the a3/4 element controlling *Mhrt* (Extended Data Fig. 4a). On a1 and a3/4 (but not a2), we found cardiac-specific enrichment of Brg1 (ref. 3), H3K4me3 and H3K36me3 (Extended Data Fig. 4c–d), and DNaseI genomic footprints (Fig. 3a)[22]. To test a3/4 for *Mhrt* regulation, we conducted deletional analysis of the a1–a4 promoter in the *Mhrt* transcription direction. In reporter assays, a3/4 was necessary and sufficient for *Mhrt* promoter activity and for Brg1-dependent *Mhrt* repression, whereas a1 was not essential for either (Extended Data Fig. 4h). Conversely, a1 is necessary and sufficient for Brg1 to repress the *Myh6* promoter[3], but a3/4 is not required[3]. Therefore, a1 and a3/4 are two functionally distinct elements for Brg1 to separately control *Myh6* and *Mhrt*.

In stressed hearts, Brg1 represses *Myh6* and activates *Myh7* (ref. 3), causing a pathological switch of *Myh6/7* expression, contributing to cardiomyopathy[23]. This stress/Brg1-dependent *Myh* switch was largely eliminated by *Mhrt779* (Fig. 3b), and the inhibition of the *Myh* switch by *Mhrt* did not involve RNA–RNA sequence interference between *Mhrt* and *Myh* (Extended Data Fig. 5a–j and Supplementary Note). Instead, it required a physical interaction between *Mhrt* RNA and Brg1. RNA immunoprecipitation of TAC-stressed adult hearts or Brg1-expressing neonatal hearts showed that Brg1 co-immunoprecipitated with *Mhrt779* but not control RNAs, and that *Mhrt779* complexed with Brg1 but not with the polycomb proteins Ezh2 or Suz12 (Fig. 3c and Extended Data Fig. 6a, b). The Brg1–*Mhrt* complex was minimal in unstressed adult hearts with low Brg1 (ref. 3) or in stressed *Brg1*-null hearts (*Tnnt-rtTA; Tre-Cre;Brg1*$^{fl/fl}$)[3] (Fig. 3c and Supplementary Note). These results suggest that *Mhrt* binds to Brg1 to influence its gene regulation.

We then tested how *Mhrt* regulated Brg1 activity on its *in vivo* target genes, including *Myh6* (ref. 3), *Myh7* (ref. 3) and *Opn* (osteopontin, critical for cardiac fibrosis[12]) (Extended Data Fig. 6c–e and Supplementary Note). In doxycycline-treated, TAC-stressed *Tg799* hearts, *Mhrt779*—without affecting the Brg1 messenger RNA/protein level (Extended Data Fig. 7a–f)—reduced Brg1 occupancy on *Myh6*, *Myh7* and *Opn* promoters by 60–90% (Fig. 3d), causing a 56–76% loss of Brg1-controlled *Myh* switch and *Opn* activation (Fig. 3b and Extended Data Figs 6e, 7g). We then used primary rat ventricular cardiomyocytes to conduct reporter assays. In these cells, as observed *in vivo*, Brg1 repressed *Myh6* and activated *Myh7* and *Opn* promoters; *Mhrt779* reduced Brg1 activity on these promoters by 54–80% (Fig. 3e). Accordingly, *Mhrt* prevents Brg1 from binding to its genomic targets to control gene expression.

How Brg1 or ATP-dependent chromatin remodellers recognize their target promoters is an important but not fully understood issue in chromatin biology. Biochemically, recombinant Brg1 proteins and *in vitro* transcribed *Mhrt779* could directly co-immunoprecipitate without involving other factors (Fig. 3f). An electrical mobility shift assay (EMSA) showed that Brg1 shifted biotin-labelled *Mhrt779* to form a low mobility

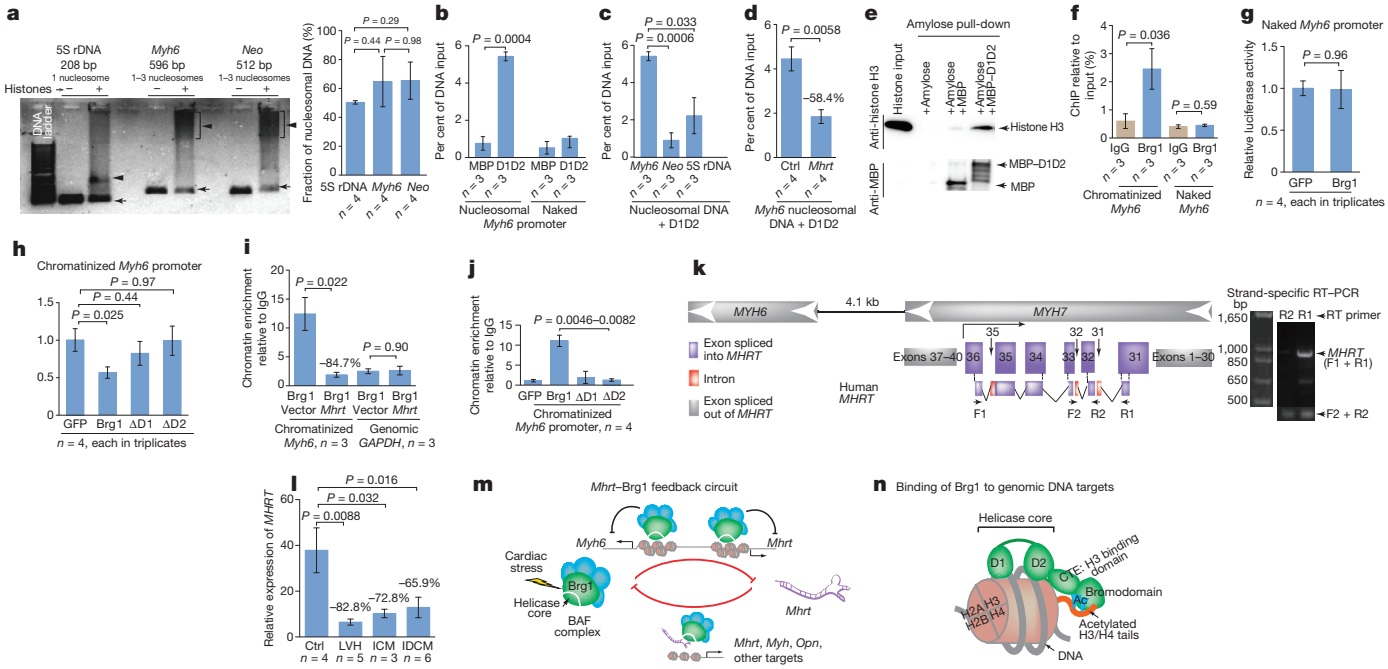

Figure 4 | *Mhrt* inhibits chromatin targeting and gene regulation by Brg1. **a**, Gel electrophoresis and quantification of nucleosomal 5S rDNA, the *Myh6* promoter and *Neo* DNA. Arrowheads indicate the DNA–histone complex; arrows indicate naked DNA. Nucleosome assembly efficiency is defined as the fraction of DNA bound to histones (arrowheads). **b**–**d**, Quantification of amylose pull-down of MBP–D1D2 (D1D2) with nucleosomal and naked *Myh6* promoter DNA (**b**), with nucleosomal *Myh6* promoter, *Neo* and 5S rDNA (**c**), or with nucleosomal *Myh6* promoter in the presence of *Mhrt779* (**d**). **e**, Amylose pull-down of MBP–D1D2 and histone H3. Anti-histone H3 and anti-MBP antibodies were used for western blot analysis. **f**, ChIP analysis of Brg1 on chromatinized and naked *Myh6* promoter in rat ventricular cardiomyocytes. GFP, green fluorescent protein control. **g**, **h**, Luciferase reporter activity of Brg1 on naked *Myh6* promoter (**g**) or of helicase-deficient Brg1 on chromatinized *Myh6* promoter (**h**) in rat ventricular cardiomyocytes. ΔD1, Brg1 lacking amino acid 774–913; ΔD2, Brg1 lacking 1086–1246. ChIP: H-10 antibody recognizing N terminus, non-disrupted region of Brg1. **i**, **j**, ChIP analysis in SW13 cells of chromatinized *Myh6* promoter in the presence of *Mhrt779* (**i**) or helicase-deficient Brg1 (**j**). *Mhrt*, pAdd2-*Mhrt779*; Vector, pAdd2 empty vector. **k**, Schematic illustration and PCR of human *MHRT*. *MHRT* originates from *MYH7* and is transcribed into *MYH7*. *MYH7* exons and introns are indicated. R1 and R2 are strand-specific primers; F1 and R1 target *MHRT* and *MYH7*; F2 and R2 are specific for *MHRT*. **l**, Quantification of *MHRT* in human heart tissues. Ctrl, control; ICM, ischaemic cardiomyopathy; IDCM, idiopathic dilated cardiomyopathy; LVH, left ventricular hypertrophy. **m**, Working model of a Brg1–*Mhrt* feedback circuit in the heart. Brg1 represses *Mhrt* transcription, whereas *Mhrt* prevents Brg1 from recognizing its chromatin targets. Brg1 functions through two distinct promoter elements to bidirectionally repress *Myh6* and *Mhrt* expression. **n**, Molecular model of how Brg1 binds to its genomic DNA targets. Brg1 helicase (D1D2) binds chromatinized DNA, C-terminal extension (CTE) binds histone H3, and bromodomain binds acetylated histone H3 or H4. *P* values: Student's *t*-test. Error bars show s.e.m.

protein–RNA complex that was competitively disrupted by unlabelled *Mhrt779* (Fig. 3f). Brg1, which belongs to the SWI/SNF family of chromatin-remodelling factors, contains a helicase/ATPase core that is split by an insertion into two RecA-like domains: DEAD-like helicase superfamily C-terminal domain, D1 (DExx-c) and helicase superfamily C-terminal domain, D2 (HELIC-c)[24,25], with signature motifs of DEAD-box, superfamily 2 RNA helicase[25,26] (Fig. 3g and Extended Data Fig. 8). SWI/SNF proteins although conserved with RNA helicases, were observed to bind DNA[27] and mediate DNA structural changes and repair[19]. The binding properties of Brg1 remained undefined. To test whether *Mhrt* could bind to Brg1 helicase, we generated maltose-binding protein (MBP)-tagged recombinant proteins that contained the Brg1 DExx-c domain (MBP–D1, amino acids 774–913), the HELIC-c domain with C-terminus extension (MBP–D2, 1086–1310), or the entire helicase (MBP–D1D2, 774–1310) (Extended Data Fig. 9a). D1D2 showed the highest *Mhrt* binding affinity (dissociation constant (K_d) = 0.76 μM); D1 showed moderate affinity (K_d = 1.8 μM); D2 modest affinity (K_d > 150 μM); and MBP did not bind at all (Fig. 3h, i). Therefore, Brg1 helicase binds *Mhrt* with high affinity.

Contrary to its potent RNA binding, Brg1 helicase showed no detectable binding to the naked DNA of the *Myh6* promoter (596 bp, −426 to +170, critical for the control of *Myh6* by Brg1 (ref. 3)) (Extended Data Fig. 9b). To test whether Brg1 helicase could bind chromatinized DNA, we generated nucleosomal DNA *in vitro* by assembling histone octamers (histones H2A, H2B, H3 and H4)[28] on *Myh6* promoter DNA, as well as on control neomycin phosphotransferase gene (*Neo*) and 5S ribosomal (r)DNA (5S rDNA). We achieved 50–65% efficiency of nucleosome assembly, comparable between *Myh6*, *Neo* and 5S rDNA (Fig. 4a). Because the large nucleosome size precluded a clear EMSA resolution, we used amylose to pull down MBP-tagged D1D2 proteins. We found that D1D2 pulled down nucleosomal *Myh6* promoter DNA but not the naked one (Fig. 4b). The pull-down efficiency of nucleosomal *Myh6* was ~3–6-fold that of *Neo* or 5S rDNA (Fig. 4c), and *Mhrt779* was capable of disrupting D1D2–*Myh6* pull-down (Fig. 4d). Although D1D2 bound to histone H3 (Fig. 4e), histone binding was insufficient to anchor D1D2 to nucleosomal DNA, as D1D2 bound poorly to nucleosomal *Neo* and 5S rDNA that also contained histones (Fig. 4c). Therefore, chromatinized DNA targets are biochemically recognized by Brg1 helicase, and this process is inhibited by *Mhrt*.

To test the ability of Brg1 to distinguish chromatinized from naked DNA promoters in cells, we cloned *Myh6* promoter into the luciferase reporter plasmid pREP4 (allowing promoter chromatinization[19]) and pGL3 (containing naked, non-chromatinized promoter). In rat ventricular cardiomyocytes and SW13 cells, ChIP and luciferase analyses showed that Brg1 bound and repressed chromatinized but not naked *Myh6* promoter (Fig. 4f, g and Extended Data Fig. 9c, d). However, without D1/D2 domain or in the presence of *Mhrt*, Brg1 was unable to bind or repress chromatinized *Myh6* promoter (Fig. 4h–j and Extended Data Fig. 9e), indicating the necessity of D1D2 for the interaction between Brg1, chromatin and *Mhrt*. Consistently, all our genetic, biochemical and cellular

studies show that Brg1 requires the helicase domain to bind to chromatinized DNA targets, and *Mhrt* seizes the helicase to disrupt Brg1–chromatin binding.

We then asked how Brg1 surpassed its basal suppression by *Mhrt* to control *Myh*, *Mhrt*, *Opn*, or other genes to trigger cardiomyopathy (Supplementary Note). Amylose pull-down experiments showed that Brg1 dose-dependently escaped from *Mhrt* inhibition to occupy *Mhrt* promoter (Extended Data Fig. 10). Brg1 protein, which increases under stress conditions[3], could therefore outrun *Mhrt* and gain control over the *Mhrt* promoter to repress *Mhrt* expression and tip the balance towards Brg1. Contrary to the endogenous *Mhrt* that was repressible by Brg1, the *Mhrt* transgene (*Tg779*)—driven by *Tnnt2*/*Tre* promoters—was not subject to repression by Brg1 and was thus able to keep *Mhrt* at pre-stress levels to inhibit Brg1 and reduce hypertrophy. This further demonstrates the necessity of *Mhrt* repression for myopathy to develop.

Human *MYH7* loci encoded RNA that resembled *Mhrt* in primary sequence and secondary structure, as predicted by minimal free energy[29] (Fig. 4k and Extended Data Fig. 11a, b). Human *MHRT* was also repressed in stressed hearts, with 82.8%, 72.8% and 65.9% reduction of *MHRT* in hypertrophic, ischaemic or idiopathic cardiomyopathy tissues, respectively (Fig. 4l and Extended Data Fig. 11c). This suggests a conserved *MHRT* mechanism of human cardiomyopathy.

Mhrt is the first example, to our knowledge, of a lncRNA that inhibits myopathy and chromatin remodellers. Reciprocal *Mhrt*–Brg1 inhibition constitutes a feedback circuit critical for maintaining cardiac function (Fig. 4m). The helicase core of Brg1, combined with the histone-binding domains of the Brg1/BAF complex, adds a new layer of specificity control to Brg1/BAF targeting and chromatin remodelling (Fig. 4n). The *Mhrt*–helicase interaction also exemplifies a new mechanism by which lncRNA controls chromatin structure. To further elucidate chromatin regulation, it will be essential to define helicase domain function in all ATP-dependent chromatin-remodelling factors and to identify new members of lncRNA that act through this domain to control chromatin. The cardioprotective *Mhrt* may have translational value, given that RNA can be chemically modified and delivered as a therapeutic drug. This aspect of lncRNA–chromatin regulation may also inspire new therapies for human disease.

METHODS SUMMARY

Tg779 mouse generation, rapid amplification of cDNA ends (RACE), RNA *in situ* hybridization, RT–qPCR, codon substitution frequencies (CSF), echocardiography, northern blot, EMSA, ChIP, RNA immunoprecipitation, reporter assay, nucleosome assembly, and the amylose pull-down assay were performed as described[3,4,28].

Online Content Methods, along with any additional Extended Data display items and Source Data, are available in the online version of the paper; references unique to these sections appear only in the online paper.

Received 25 March 2013; accepted 17 June 2014.

Published online 10 August; corrected online 1 October 2014 (see full-text HTML version for details).

1. RIKEN Genome Exploration Research Group and Genome Science Group (Genome Network Project Core Group) and the FANTOM Consortium. Antisense transcription in the mammalian transcriptome. *Science* **309,** 1564–1566 (2005).
2. Haddad, F., Bodell, P. W., Qin, A. X., Giger, J. M. & Baldwin, K. M. Role of antisense RNA in coordinating cardiac myosin heavy chain gene switching. *J. Biol. Chem.* **278,** 37132–37138 (2003).
3. Hang, C. T. *et al.* Chromatin regulation by Brg1 underlies heart muscle development and disease. *Nature* **466,** 62–67 (2010).
4. Hung, T. *et al.* Extensive and coordinated transcription of noncoding RNAs within cell-cycle promoters. *Nature Genet.* **43,** 621–629 (2011).
5. Lin, M. F., Jungreis, I. & Kellis, M. PhyloCSF: a comparative genomics method to distinguish protein coding and non-coding regions. *Bioinformatics* **27,** i275–i282 (2011).
6. Ingolia, N. T., Brar, G. A., Rouskin, S., McGeachy, A. M. & Weissman, J. S. The ribosome profiling strategy for monitoring translation *in vivo* by deep sequencing of ribosome-protected mRNA fragments. *Nature Protocols* **7,** 1534–1550 (2012).
7. van Rooij, E. *et al.* Control of stress-dependent cardiac growth and gene expression by a microRNA. *Science* **316,** 575–579 (2007).
8. Miyata, S., Minobe, W., Bristow, M. R. & Leinwand, L. A. Myosin heavy chain isoform expression in the failing and nonfailing human heart. *Circ. Res.* **86,** 386–390 (2000).
9. Lompre, A. M. *et al.* Myosin isoenzyme redistribution in chronic heart overload. *Nature* **282,** 105–107 (1979).
10. Schultz, J. J. *et al.* TGF-β1 mediates the hypertrophic cardiomyocyte growth induced by angiotensin II. *J. Clin. Invest.* **109,** 787–796 (2002).
11. Molkentin, J. D. & Dorn, G. W. II. Cytoplasmic signaling pathways that regulate cardiac hypertrophy. *Annu. Rev. Physiol.* **63,** 391–426 (2001).
12. López, B. *et al.* Osteopontin-mediated myocardial fibrosis in heart failure: a role for lysyl oxidase? *Cardiovasc. Res.* **99,** 111–120 (2013).
13. Frey, N. & Olson, E. N. Cardiac hypertrophy: the good, the bad, and the ugly. *Annu. Rev. Physiol.* **65,** 45–79 (2003).
14. Guttman, M. *et al.* Chromatin signature reveals over a thousand highly conserved large non-coding RNAs in mammals. *Nature* **458,** 223–227 (2009).
15. Rando, O. J. & Chang, H. Y. Genome-wide views of chromatin structure. *Annu. Rev. Biochem.* **78,** 245–271 (2009).
16. Hahn, M. A., Wu, X., Li, A. X., Hahn, T. & Pfeifer, G. P. Relationship between gene body DNA methylation and intragenic H3K9me3 and H3K36me3 chromatin marks. *PLoS ONE* **6,** e18844 (2011).
17. Mikkelsen, T. S. *et al.* Genome-wide maps of chromatin state in pluripotent and lineage-committed cells. *Nature* **448,** 553–560 (2007).
18. Musselman, C. A. *et al.* Molecular basis for H3K36me3 recognition by the Tudor domain of PHF1. *Nature Struct. Mol. Biol.* **19,** 1266–1272 (2012).
19. Liu, R. *et al.* Regulation of CSF1 promoter by the SWI/SNF-like BAF complex. *Cell* **106,** 309–318 (2001).
20. Muchardt, C. & Yaniv, M. A human homologue of *Saccharomyces cerevisiae* SNF2/SWI2 and *Drosophila brm* genes potentiates transcriptional activation by the glucocorticoid receptor. *EMBO J.* **12,** 4279–4290 (1993).
21. Szabó, G. *et al.* Poly(ADP-ribose) polymerase inhibition reduces reperfusion injury after heart transplantation. *Circ. Res.* **90,** 100–106 (2002).
22. Hesselberth, J. R. *et al.* Global mapping of protein–DNA interactions *in vivo* by digital genomic footprinting. *Nature Methods* **6,** 283–289 (2009).
23. Gupta, M. P. Factors controlling cardiac myosin-isoform shift during hypertrophy and heart failure. *J. Mol. Cell. Cardiol.* **43,** 388–403 (2007).
24. Clapier, C. R. & Cairns, B. R. The biology of chromatin remodeling complexes. *Annu. Rev. Biochem.* **78,** 273–304 (2009).
25. Jankowsky, E. & Fairman, M. E. RNA helicases—one fold for many functions. *Curr. Opin. Struct. Biol.* **17,** 316–324 (2007).
26. Mallam, A. L., Del Campo, M., Gilman, B., Sidote, D. J. & Lambowitz, A. M. Structural basis for RNA-duplex recognition and unwinding by the DEAD-box helicase Mss116p. *Nature* **490,** 121–125 (2012).
27. Dürr, H., Korner, C., Muller, M., Hickmann, V. & Hopfner, K. P. X-ray structures of the *Sulfolobus solfataricus* SWI2/SNF2 ATPase core and its complex with DNA. *Cell* **121,** 363–373 (2005).
28. Feng, Y. *et al.* Histone H4 acetylation differentially modulates arginine methylation by an in *cis* mechanism. *J. Biol. Chem.* **286,** 20323–20334 (2011).
29. Zuker, M. On finding all suboptimal foldings of an RNA molecule. *Science* **244,** 48–52 (1989).

Supplementary Information is available in the online version of the paper.

Acknowledgements We thank C.-H. Chen for assisting with echocardiography; L. Chen, A. Kuo and G. Crabtree for transgene injection and northern blot; M. Ecarkt and E. Zuo for ribosome analysis. C.-P.C. was supported by the American Heart Association (AHA; Established Investigator Award 12EIA8960018), National Institutes of Health (NIH; HL118087, HL121197), March of Dimes Foundation (#6-FY11-260), California Institute of Regenerative Medicine (CIRM; RN2-00909), Oak Foundation, Baxter Foundation, Stanford Heart Center Research Program, Indiana University (IU) School of Medicine—IU Health Strategic Research Initiative, and the IU Physician-Scientist Initiative, endowed by Lilly Endowment. W.L. and Y.X. were supported by the Oak Foundation; Y.X. by the AHA and Lucile Packard Children's Foundation; C.S. by an NIH fellowship; T.Q. by NIH (HL109512); H.-S.V.C. by CIRM (RB2-01512, RB4-06276) and NIH (HL105194); P.-S.C. by NIH (HL78931, HL71140); B.Z. by NIH (HL116997, HL111770).

Author Contributions C.-P.C. and P.H. were responsible for the original concepts, design and manuscript preparation. W.L. and C.-H.L. contributed equally to the work. P.H. conducted most experiments; W.L. and J.Y. assisted with TAC, echo and reporter analyses; C.-H.L. assisted with protein purification; S.T.N. assisted with ribosome data analysis; K.K.J. assisted with protein sequence and motif analysis; C.S. assisted with western blot studies; W.X. assisted with CSF scoring; Y.X. assisted with RNA/protein staining; C.-J.L. and C.-Y.L. assisted with *Brg1*-null tissue preparation and H-10 antibody-ChIP optimization; H.-C.C. assisted with cloning; H.-S.V.C. assisted with tissue collection; E.A. assisted with tissue collection/rat tissue supply; B.Z. assisted with driver line generation; D.B., P.-S.C. and T.Q. assisted with data analysis.

Author Information Data have been deposited in the Gene Expression Omnibus under accession number GSE49716. Reprints and permissions information is available at www.nature.com/reprints. The authors declare no competing financial interests. Readers are welcome to comment on the online version of the paper. Correspondence and requests for materials should be addressed to C.-P.C. (changcp@iu.edu).

METHODS

Mice, animal sample size, and randomization. For the generation of *Tg779* mice, *Mhrt779* was cloned into the pTRE2 backbone (Clonetech). A DNA fragment containing the Tre promoter and *Mhrt779* were injected into the pronucleus of fertilized oocytes (B6C3H/F1). Embryos were implanted into a pseudopregnant CD-1 mouse. The *Tre-Mhrt779* transgene was identified by PCR genotyping using primers CGCCTGGAGACGCCATCCAC and TGTCTTCAAAGCTGACTCCCT. *Tre-Mhrt779* mice with ~3 copies of the transgene were backcrossed with *Tnnt2-rtTA* mice as described previously[3,30] to generate *Tnnt2-rtTA;Tre-Mhrt779* (*Tg779*) mice. The number of animals used (*n*) is denoted in each test in the figures, including technical replicates when applicable. We routinely used mouse littermates to control and perform our experiments. Each subgroup of experiments had $n = 3$ to 14 biological replicates, many of which had technical replicates of three. Assignment to each experimental subgroup was based on genotypes. Littermate mice with the same genotypes regardless of gender were randomly selected from the cage and assigned to different control and experimental subgroups. Major procedures were blinded. The use of mice for studies was in compliance with the regulations of Indiana University, Stanford University and the National Institutes of Health.

RACE and cloning of full length of *Mhrt* transcripts. The 3′ and 5′ RACE were performed using the FirstChoice RLM-RACE Kit (Ambion) following the manufacturer's instruction. RNA was extracted from adult heart ventricles. Primers used for 3′ and 5′ RACE were designed based on the known sequence information: TC ATTGGCACGGACAGCATC (first-round *Mhrt* 3′-prime specific) and GAGCA TTTGGGGATGGTATAC (second-round *Mhrt* 3′-prime specific); CAACACTT TTCATTTTCCTCTTT (first-round *Mhrt* 5′-prime specific) and TCTGCTTCA TTGCCTCTGTTT (second-round *Mhrt* 5′-prime specific). Once we reached the 5′ and 3′ cDNA ends, we used primers F1 (Fig. 1a; AAGAGCCCTACAGTCTG ATGAACA) and R1 (Fig. 1a; CCTTCACACAAACATTTTATTT) to amplify the full-length *Mhrt* transcripts and cloned them into pDrive TA cloning vector (Qiagen) for sequencing. *Mhrt* RNAs were also further cloned into shuttle vector pAdd2 (refs 31, 32) for expression in cells.

Northern blot and *in situ* hybridization. We obtained 5 μg of total RNA using Quick-RNA Mini Kit (Zymo Research). RNA blot was performed using NorthernMax Kit (Ambion) following the manufacturer's protocol. Single-stranded RNA probe was generated by *in vitro* transcription with MaxIscript SP6/T7 kit (Ambion) with ATP [α-^{32}P] (PerkinElmer) using full-length *Mhrt779*, *Myh6* and *Myh7* as the template and followed by digestion with DNase I (Ambion). Hybridization was performed at 65 °C. The blot was washed and imaged by Phosphor storage scanning by Typhoon 8600 Imager (GE Healthcare). *In situ* hybridization experiments were performed as previously described[3,33].

RNA fractionation. To isolate cytosolic and nuclear RNAs from adult heart tissues, we used a PARIS kit (Ambion) and followed the manufacturer's instruction. Ten milligrams of tissue were homogenized in cell fractionation buffer thoroughly before centrifuging for 5 min at 500*g*. Supernatant was collected as the cytosolic fraction, while the nuclear pellet was washed and lysed by cell disruption buffer. Such samples were further mixed with 2× lysis/binding solution before extracting RNA using the manufacturer's protocol.

Codon substitution frequency predication. To measure the coding potential of *Mhrt*, we used the previously described codon substitution frequencies (CSF) method[4,5] to evaluate the evolutionary characteristics in their alignments with orthologous regions in six other sequenced mammalian genomes (rat, human, hamster, rhesus monkey, cat and dog). CSF generates a likelihood score for a given sequence considering all codon substitutions observed within its alignment across multiple species, which was based on the relative frequency of similar substitutions occurring in known coding and noncoding regions. CSF compares two empirical codon models; one generated from alignments of known coding regions and the other according to noncoding regions, producing a likelihood ratio. The ratio reflects whether the protein-coding model better explains the alignment.

Ribosome profiling and RNA deep sequencing. For ribosome profiling[6], overexpression of the predominant species of *Mhrt* (*Mhrt779*) along with *HOTAIR* were achieved through co-transfecting pAdd2-779 and pAdd2-HOTAIR into SW13 cells. The cells were then lysed to extract ribosome-associated RNA fragments using ARTseq Ribosome Profiling Kit (Epicentre, Illumina). The RNA fragments were further converted into a DNA library through end repair, adaptor ligation, reverse transcription circularization, and PCR amplification. A conventional RNA-seq library was also prepared, with total RNA extracted from those cells with an miRNeasy Mini Kit (Qiagen #217004). The libraries were further processed according to an MiSeq Sample Prep sheet, and an MiSeq 50 cycle kit was used for sequencing. PCR products (1.25 pmol) were used for sequencing. Approximately 600,000–700,000 reads were properly paired and used for further analysis. The resulting reads were aligned to the human hg19 or mouse mm10 genome using Bowtie2 v.2.0.0.6 (ref. 34). Mapped reads were visualized on the UCSC browser as bigwig files generated using samtools v.0.1.18 (ref. 35), bedtools v.2.16.1 (ref. 36), bedClip and bedGraphToBigWig. For quantification of fragments per kilobase of exon per million fragments mapped (FPKM) values, cuffdiff as part of the tophat suite v.2.0.8b[37] was run on a merged bam file containing the human and the *Mhrt* reads using a custom gtf file comprising the human hg19 iGenome and the *Mhrt* transcripts. To generate scatter plots of the genes, cuffdiff files were used for visualization with cummerbund v.2.3.1 (ref. 37).

***In vitro* translation and biotin labelling.** TNT Quick Coupled Transcription/Translation System (Promega) was used for *in vitro* translation. Briefly, 1 μg plasmids of control (luciferase) and various *Mhrt* species inserted into pDrive vector were added to 40 μl rabbit reticulocyte lysates containing ^{35}S-methionine. After 1 h of incubation, the reactions were analysed on 10–20% Tris-Tricine gel. The gel was dried and visualized by the Typhoon 8600 Imager (GE Healthcare). Biotin-NTP was added to the *in vitro* translation reaction. Total RNAs were extracted and the biotin-labelled RNAs were detected subsequently by IRDye 680 Streptavidin (LiCOR, 926-68079) using an Odyssey Infrared Imaging System.

TAC. The TAC surgery was performed as described[3] on adult mice of 8–10 weeks of age and between 20 and 25 g in weight. Mice were fed with doxycycline food pellets (6 mg doxycycline per kg of food; Bioserv) 7–14 days before the TAC operation. Mice were anaesthetized with isoflurane (2–3%, inhalation) in an induction chamber and then intubated with a 20-gauge intravenous catheter and ventilated with a mouse ventilator (Minivent, Harvard Apparatus). Anaesthesia was maintained with inhaled isoflurane (1–2%). A longitudinal 5 mm incision of the skin was made with scissors at the midline of sternum. The chest cavity was opened by a small incision at the level of the second intercostal space 2–3 mm from the left sternal border. While opening the chest wall, the chest retractor was gently inserted to spread the wound 4–5 mm in width. The transverse portion of the aorta was bluntly dissected with a curved forceps. Then, 6-0 silk was brought underneath the transverse aorta between the left common carotid artery and the brachiocephalic trunk. One 27-gauge needle was placed directly above and parallel to the aorta. The loop was then tied around the aorta and needle, and secured with a second knot. The needle was immediately removed to create a lumen with a fixed stenotic diameter. The chest cavity was closed by 6-0 silk suture. Sham-operated mice underwent similar surgical procedures, including isolation of the aorta and looping of the aorta, but without tying of the suture. The pressure load caused by TAC was verified by the pressure gradient across the aortic constriction measured by echocardiography. Only mice with a pressure gradient >30 mm Hg were analysed for cardiac hypertrophy, echocardiography and other purposes.

Echocardiography. The echocardiographer was blinded to the genotypes and surgical procedure. Transthoracic ultrasonography was performed with a GE Vivid 7 ultrasound platform (GE Health Care) and a 13 MHz transducer was used to measure aortic pressure gradient and left ventricular function. Echocardiography was performed on control and *Tnnt2-rtTA;Tre-Mhrt779* (*Tg779*) mice at designated time points after the TAC procedure. To minimize the confounding influence of different heart rates on the aortic pressure gradient and left ventricular function, the flow of isoflurane (inhalational) was adjusted to anaesthetize the mice while maintaining their heart rates at 450–550 beats per minute. The peak aortic pressure gradient was measured by continuous-wave Doppler across the aortic constriction. Left ventricular function was assessed by M-mode scanning of the left ventricular chamber, standardized by two-dimensional, short-axis views of the left ventricle at the mid papillary muscle level. Left ventricular chamber size and wall thickness were measured in at least three beats from each projection and averaged. Left ventricular internal dimensions at diastole and systole (LVIDd and LVIDs, respectively) were measured. The fractional shortening (FS) of the left ventricle was defined as $100\% \times (1 - \text{LVIDs/LVIDd})$, representing the relative change of left ventricular diameters during the cardiac cycle. The mean FS of the left ventricle was determined by the average of FS measurements of the left ventricular contraction over five beats. *P* values were calculated by Student's *t*-test. Error bars indicate s.e.m.

Histology, trichrome staining and morphometric analysis of cardiomyocytes. Histology and trichrome staining were performed as described[38,39]. Trichrome stain (Masson) kit (Sigma) was used and the manufacturer's protocol was followed. For morphometric analysis of cardiomyocytes, paraffin sections of the heart were immunostained with a fluoresecin isothiocyanate-conjugated wheat germ agglutinin (WGA) antibody (F49, Biomeda) that highlighted the cell membrane of cardiomyocytes. Cellular areas outlined by WGA were determined by the number of pixels enclosed using ImageJ software (NCBI). Approximately 250 cardiomyocytes of the papillary muscle at the mid-left ventricular cavity were measured to determine the size distribution. *P* values were calculated by Student's *t*-test. Error bars indicate s.e.m.

RT–qPCR and strand-specific reverse transcription PCR analysis. RT–qPCR analyses were performed as described[3,38]. The following primer sequences (listed later) were used. RT–qPCR reactions were performed using SYBR green master mix (BioRad) with an Eppendorf realplex, and the primer sets were tested to be quantitative. Threshold cycles and melting curve measurements were performed with software. *P* values were calculated by Student's *t*-test. Error bars indicate s.e.m. To conduct strand-specific RT–PCR analysis, human total RNA and Superscript III First-Strand

Synthesis System (Invitrogen) was used. Primers R1 (Fig. 4k; CTACAGAATGAG ATCGAGGACT) and R2 (Fig. 4k; GGGGCTGAAGAGTGAGCCTT) were designed based on known sequence and were used for individual RTs, respectively. To detect *MHRT*, primers F1 (Fig. 4k; CTGGAGCTGGGACAGGTCAGCA) and R1 were used. These primers could also amplify endogenous *MYH7* and thus serve as controls. Primers F2 (Fig. 4k; TGGGGAACACGGCGTTCTTGA) and R2 were used to specifically amplify *MHRT* and used in RT–qPCR analysis.

PCR primers for RT–qPCR of mRNA were as follows. Mouse *TfIIb*-F, CTCTG TGGCGGCAGCAGCTATTT, mouse *TfIIb*-R,CGAGGGTAGATCAGTCTGTA GGA; mouse *Hprt1*-F, GCTGGTGAAAAGGACCTCT, mouse *Hprt1*-R, CACAG GACTAGAACACCTGC; mouse *Anf*-F, GACTAGGCTGCAACAGCTTCCG, mouse *Anf*-R, GCCACAGTGGCAATGTGACCAA; mouse *Serca2a*-F, CATTTG CATTGCAGTCTGGAT, mouse *Serca2a*-R, CTTTGCCATCCTACGAGTTCC; mouse *Tnnt2*-F, TACAGACTCTGATCGAGGCTCACTTC, mouse *Tnnt2*-R, TC ATTGCGAATACGCTGCTGCTC; mouse *Mhrt*-F (common), GAGCATTTGG GGATGGTATAC, mouse *Mhrt*-R (common), TCTGCTTCATTGCCTCTGTT T; mouse *Mhrt779*-F, TCTGGCCACAGCCCGCAGCTTC, mouse *Mhrt779*-R, AGTCATGTATACCATCCCCAA; Mouse *Neat1*-F, TCTCCTGGAGCCACATC TCT, mouse *Neat1*-R, GCTTTTCCTTAGGCCCAAAC; mouse 28S-rRNA-F, GG TAGCCAAATGCCTCGTCAT, mouse 28S-rRNA-R, CCCTTGGCTGTGGTTT CG; human *TFIIB*-F, ACCACCCCAATGGATGCAGACAG, human *TFIIB*-F, A CGGGCTAAGCGTCTGGCAC; human *MHRT*-F (F2), TGGGGAACACGGCG TTCTTGA, human *MHRT*-R (R2), GGGGCTGAAGAGTGAGCCTT; human *HOTAIR*-F, GGTAGAAAAAGCAACCACGAAGC, human *HOTAIR*-R, ACAT AAACCTCTGTCTGTGAGTGCC; human *GAPDH*-F, CCGGGAAACTGTGG CGTGATGG, human *GAPDH*-R, AGGTGGAGGAGTGGGTGTCGCTGTT.

ChIP–qPCR. ChIP assay was performed as described[3] with modifications. Briefly, chromatin from hearts or SW13 cells was sonicated to generate average fragment sizes of 200–600 bp, and immunoprecipitated using anti-BRG1 J1 antibody[3,40], anti-Brg1 H-10 antibody (Santa Cruz Biotechnology, against 115–149 amino acids of N terminus Brg1), anti-RNA polymerase II (Pol II) antibody (ab24759, Abcam), anti-H3K4me3 antibody (07-473, Millipore), anti-H3K36me3 antibody (17-10032, Millipore) or normal control IgG. Isolation and purification of immunoprecipitated and input DNA were done according to the manufacturer's protocol (Magna ChIP Protein G Magnetic Beads, Millipore), and qPCR analysis of immunoprecipitated DNA were performed. ChIP–qPCR signal of individual ChIP reactions was standardized to its own input qPCR signal or IgG ChIP signal. PCR primers (listed later) were designed to amplify the promoter regions of mouse *Myh6* (−426, −320), mouse *Myh7* (−102, +58), mouse *Shh* (−7142, −6911), mouse *Vegfa* (+1, +150) human *GAPDH* (−45, +121). The DNA positions are denoted relative to the transcriptional start site (+1).

PCR primers for ChIP–qPCR are as follows. Mouse ChIP-*Myh6* promoter-F, GCAGATAGCCAGGGTTGAAA, mouse ChIP-*Myh6* promoter-R, TGGGTAA GGGTCACCTTCTC; mouse ChIP-*Myh7* promoter-F, GTGACAACAGCCCT TTCTAAAT, mouse ChIP-*Myh7* promoter-R, CTCCAGCTCCCACTCCTACC; mouse ChIP-*Shh* promoter-F, GAGAACATTACAGGGTAGGAA, mouse ChIP-*Shh* promoter-R, GAAGCAGTGAGGTTGGTGG; mouse ChIP-*Vegfa* promoter-F, CAAATCCCAGAGCACAGACTC, mouse ChIP-*Vegfa* promoter-R, AGCGCAG AGGCTTGGGGCAGC; human ChIP-*GAPDH* promoter-F, TACTAGCGGTTTT ACGGGCG, human ChIP-*GAPDH* promoter-R, TCGAACAGGAGGAGCAGAG AGCGA.

RNA immunoprecipitation. RNA immunoprecipitation (RNA-IP, RIP) was conducted as described[4] with some modifications. Briefly, P1 hearts, sham hearts or those from mice that had undergone TAC, or SW13 cells were crosslinked and lysed with lysis buffer (10 mM HEPES pH 7.5, 85 mM KCl, 0.5% NP-40, 1 mM dithiothreitol (DTT), 1× protease inhibitor) for tissues or lysis buffer (10 mM Tris-HCl pH 8.1, 10 mM NaCl, 1.5 mM $MgCl_2$, 0.5% NP-40, 1 mM DTT, 1× protease inhibitor) for cells. Nuclei were isolated and sonicated using Bioruptor (Diagenode) (30 s on, 30 s off, power setting H, 5 min, performed twice) in nuclear lysis buffer (50 mM Tris-HCl pH 8.1, 150 mM NaCl, 0.1% NP-40, 1 mM DTT, protease inhibitor, ribonuclease inhibitor). The nuclear extract was collected and incubated with primary antibodies at 4 °C overnight together with Manga ChIP Protein G Magnetic Beads (Millipore). The beads were washed by wash buffer I (20 mM Tris-Hcl pH 8.1, 150 mM NaCl, 1% Triton X-100 and 0.1% SDS) three times, and wash buffer II (20 mM Tris-Hcl pH 8.1, 500 mM NaCl, 1% Triton X-100 and 0.1% SDS) three times. Beads were then resuspended in 150 µl 150 mM RIPA (50 mM Tris pH 7.5, 150 mM NaCl, 1 mM EDTA, 0.1% SDS, 1% NP-40, 0.5% sodium deoxycholate) with 5 µl Proteinase K and incubated for 1 h at 65 °C. We added 1 ml of TRIzol to the sample, and RNA was extracted using the Quick-RNA Mini Kit with the on-column DNase I digest (ZymoResearch). RT and qPCR were then conducted with the purified RNA. The antibodies used for the immunoprecipitation are anti-BRG1 J1 antibody[3,40], Ezh2 (ref. 41) (Active Motif), Suz12 (refs 41, 42) (Bethyl Laboratories) and normal IgG control.

Reporter assay and truncation of the *Mhrt* promoter. For the *Mhrt* promoter reporter assay, plasmid was constructed by inserting ~2.5 kb mouse *Mhrt* promoter into the episomal pREP4-Luc plasmid[3,19,38,43] through cloning the PCR-amplified region of the promoter by using primers ACCGGCCTGAACCCCACT TCC and ATGTCGAGACAGGGAACAGAA. Mouse *Myh6* (−426 to +170, based on new genome annotation) and *Myh7* (−3561 to +222) reporter constructs were described previously[3]. These vectors were transfected into rat neonatal cardiomyocytes or SW13 cells using lipofectamine 2000 (Invitrogen) along with plasmids expressing mouse Brg1 (actin-mBrg1-IRES-eGFP) or a matching empty vector plasmid (gifts from G. Crabtree) as well as an episomal *Renilla* luciferase plasmid (pREP7-RL) to normalize transfection efficiency. The transfected cells were cultured for 48 h and harvested for luciferase assay using the dual luciferase assay kit (Promega). For naked DNA reporter, mouse *Myh6* promoter (−426 to +170) was inserted in pGL3 vector (Promega), and *Renilla* luciferase plasmid phRL-SV40 (gifts from J. Chen) was used as a normalizer. Dual luciferase assay was performed according to the manufacturer's instruction 48 h after transfection. For deletional analysis of the *Mhrt* promoter, various regions of the promoter were deleted from the full-length pREP4-*Mhrt*. The constructs were further analysed by transfecting into SW13 cells.

RNA-EMSA and K_d calculation. Biotin-labelled RNA probe was generated by *in vitro* transcription with MAXIscript SP6/T7 kit (Ambion) with biotin labelling NTP mixture (Roche) using linearized pDrive-*Mhrt779* construct as the template and followed by digestion with DNase I (Ambion). EMSA was performed by using the LightShift Chemiluminescent RNA EMSA Kit (Thermo Scientific). The labelled probe was incubated with appropriate amounts of recombinant proteins in 10 µl in the 1× binding buffer (10 mM HEPES-KOH, pH 7.3, 10 mM NaCl, 1 mM $MgCl_2$, 1 mM DTT) with 5 µg tRNA carrier at room temperature for 30 min. The reactions were then loaded onto 1% 0.5× TBE agarose gel and transferred to BrightStar-Plus positive charged membrane. The biotin-labelled probes were detected and quantified subsequently by IRDye 680 Streptavidin (Li-COR, 926-32231) using Odyssey Infrared Imaging System. The shifted signals were quantified and plotted against amount of the MBP, MBP–D1, MBP–D2 and MBP–D1D2 proteins using a previously described method[26] with GraphPad Prism (GraphPad). The software facilitates the fitting of nonlinear regression model and calculation of K_d values based on the fitting curve. The errors and r^2 values were also generated from the fitting curve.

Protein expression and purification of Brg1 helicase domains. To generate MBP fusion proteins of mouse Brg1 helicase domains, the DExx-box domain (D1) (amino acids 774−913 of Brg1), helicase-C domain (D2) together with C-terminal extension (CTE) (amino acids 1086−1310 of Brg1), as well as the entire helicase region (D1D2) (774−1310) were amplified by PCR and cloned into pMAL vector. MBP fusion proteins were induced by isopropyl-β-D-thiogalactoside (IPTG) and purified by amylose resin (E8021S, NEB).

Nucleosome assembly and amylose pull-down. Nucleosome assembly was performed by using EpiMark Nucleosome Assembly Kit (E5350S, NEB) following the manufacturer's instruction[28]. In brief, recombinant human core histone octamer, which consists of the 2:1 mix of histone H2A/H2B dimer and histone H3.1/H4 tetramer, were mixed with purified 5S rDNA (208 bp; N1202S, NEB), *Neo* (512 bp, amplified from pST18-*Neo*; 1175025, Roche), *Myh6* core promoter (596 bp, −426 to +170) and *Mhrt* core promoter (a3/a4, 596 bp, −2290 to −1775) DNA at 2 M NaCl. PCR primers to amplify *Neo* are CGATGCGCTGCGAATCGGGA and CACTGA AGCGGGAAGGGACT. The salt concentration was gradually lowered by dilution to allow the formation of nucleosomes. The EMSA assay was used to assess the efficiency of nucleosome assembly. For amylose pull-down assay, the amylose resin (E8021S, NEB) was washed thoroughly and equilibrated with binding buffer (10 mM Tris-HCl, pH 7.5, 150 mM NaCl) before incubation with purified MBP or MBP–D1D2 proteins for 2 h. Nucleosome mixture or naked DNA mixture of 5S rDNA, *Neo* and *Myh6* promoter DNA were added for incubation at 4 °C for overnight. The resin was then washed excessively by washing buffer (20 mM Tris-HCl, pH 8.1, 150 mM NaCl, 2 mM EDTA, 1% Triton X-100, 0.1% SDS) before decross-linking and extraction of the DNA with phenol:chloroform:isoamyl alcohol. For competition assays, *in vitro* transcribed *Mhrt779* was incubated with MBP–D1D2 in binding buffer (10 mM HEPES-KOH, pH 7.3, 10 mM NaCl, 1 mM $MgCl_2$, 1 mM DTT) with ribonuclease inhibitor at room temperature for 30 min before adding nucleosomal DNA. The subsequent incubation, wash and DNA purification were performed as regular amylose pull-down assays. The qPCR signal of individual pull-down reaction was standardized to its own input RT–qPCR signal. qPCR primers were designed to amplify the 5S rDNA (CAAGCAAGAGCCTACGACCA; ATTC GTTGGAATTCCTCGGG), *Neo* (TAAAGCACGAGGAAGCGGTC; TCGACCC CAAGCGAAACAT), *Myh6* promoter (GCAGATAGCCAGGGTTGAAA; TGGG TAAGGGTCACCTTCTC) and *Mhrt* promoter (ATGCCAAATGGTTGCTCTTT; GAGCTTGAGAACCAGGCAGT).

Cloning of Brg1 truncation constructs. For cloning of truncated Brg1 with deletion of amino acids 774−913 (ΔD1) or 1086−1246 (ΔD2), primers with an NheI restriction digestion site, which complement the downstream and upstream sequences of the truncated region (ΔD1: CCCGGGGCTAGCCTGCAGAACA AGCTACCGGAGCT and CCCGGGGCTAGCCAGGTTGTTGTTGTACAGG GACA; ΔD2: CCCGGGGCTAGCATCAAGAAGTTCAAATTTCCC and CCCG GGGCTAGCCTGCAGGCCATCCTGGAGCACGAGCAG) were used to amplify from pActin-Brg1-IRES-eGFP by KOD Xtreme Hot Start DNA Polymerase (Novagen). After digestion with NheI, the linearized fragment was subject to ligation and transformation. The truncation constructs were sequenced to confirm the fidelity of the cloning. Western blot was further performed to assess the expression of the constructs. Monoclonal H-10 antibodies (Santa Cruz Biotech, sc-374197), which were raised against Brg1 N-terminal amino acids, were used in the experiments involving truncated Brg1.

Protein sequence analysis. Brg1 core helicase domain (774–1202) was applied for secondary structure prediction using the Fold & Function Assignment System (FFAS) server (http://ffas.burnham.org/ffas-cgi/cgi/ffas.pl). The output revealed that Brg1 core helicase domains are structural homologues of SF2 helicases: Vasa[44] (fruit fly, Protein Data Bank (PDB) accession number 2DB3), Rad54 (refs 27, 45) (zebrafish PDB accession 1Z3I, *Sulfolobus solfataricus* PDB accession 1Z63) and Chd1 (ref. 46) (yeast, PDB accession 3MWY). Those proteins, together with Brg1, were further employed for multiple sequence alignment with T-Coffee, which is a program allowing combination of the results obtained with several alignment methods (http://www.ebi.ac.uk/Tools/msa/tcoffee/).

RNA secondary structural prediction. To predict the secondary structure for mouse *Mhrt* and human *MHRT*, the single-stranded sequence of *Mhrt779* and human *MHRT* were analysed on the Vienna RNAfold web server (http://rna.tbi.univie.ac.at/cgi-bin/RNAfold.cgi) with calculation of minimum free energy[29,47–49].

Human heart tissue analysis. Human tissues were processed for RT–qPCR and strand-specific RT–PCR. The use of human tissues is in compliance with the regulation of Sanford/Burnham Medical Research Institute, Intermountain Medical Center, Stanford University, and Indiana University.

Primary cardiomyocyte culture. For functional studies in cardiomyocytes, neonatal rat ventricular cardiomyocytes were cultured as previously described[50,51]. Briefly, P0 or P1 Sprague–Dawley rats were used. The ventricles were excised and trypsinized for 15 min 4–5 times. Cells were then collected and resuspended in DMEM supplements with 10% FBS. The cells were plated for 1 h to allow the attachment of non-cardiomyocyte cells. The remaining cardiomyocytes were plated at a density of 2×10^5 cells ml^{-1}. The cells were transfected with Lipofectamine 2000 (Invitrogen) after 48 h.

30. Wu, B. *et al.* Inducible cardiomyocyte-specific gene disruption directed by the rat Tnnt2 promoter in the mouse. *Genesis* **48,** 63–72 (2010).
31. Wei, K., Kuhnert, F. & Kuo, C. J. Recombinant adenovirus as a methodology for exploration of physiologic functions of growth factor pathways. *J. Mol. Med. (Berl.)* **86,** 161–169 (2008).
32. Kuhnert, F. *et al.* Essential regulation of CNS angiogenesis by the orphan G protein-coupled receptor GPR124. *Science* **330,** 985–989 (2010).
33. Xiong, Y. *et al.* Brg1 governs a positive feedback circuit in the hair follicle for tissue regeneration and repair. *Dev. Cell* **25,** 169–181 (2013).
34. Langmead, B. & Salzberg, S. L. Fast gapped-read alignment with Bowtie 2. *Nature Methods* **9,** 357–359 (2012).
35. Li, H. *et al.* The Sequence Alignment/Map format and SAMtools. *Bioinformatics* **25,** 2078–2079 (2009).
36. Quinlan, A. R. & Hall, I. M. BEDTools: a flexible suite of utilities for comparing genomic features. *Bioinformatics* **26,** 841–842 (2010).
37. Trapnell, C. *et al.* Differential gene and transcript expression analysis of RNA-seq experiments with TopHat and Cufflinks. *Nature Protocols* **7,** 562–578 (2012).
38. Stankunas, K. *et al.* Endocardial Brg1 represses *ADAMTS1* to maintain the microenvironment for myocardial morphogenesis. *Dev. Cell* **14,** 298–311 (2008).
39. Chang, C. P. *et al.* A field of myocardial-endocardial NFAT signaling underlies heart valve morphogenesis. *Cell* **118,** 649–663 (2004).
40. Khavari, P. A., Peterson, C. L., Tamkun, J. W., Mendel, D. B. & Crabtree, G. R. BRG1 contains a conserved domain of the SWI2/SNF2 family necessary for normal mitotic growth and transcription. *Nature* **366,** 170–174 (1993).
41. Grote, P. *et al.* The tissue-specific lncRNA *Fendrr* is an essential regulator of heart and body wall development in the mouse. *Dev. Cell* **24,** 206–214 (2013).
42. Klattenhoff, C. A. *et al. Braveheart*, a long noncoding RNA required for cardiovascular lineage commitment. *Cell* **152,** 570–583 (2013).
43. van der Vlag, J., den Blaauwen, J. L., Sewalt, R. G., van Driel, R. & Otte, A. P. Transcriptional repression mediated by polycomb group proteins and other chromatin-associated repressors is selectively blocked by insulators. *J. Biol. Chem.* **275,** 697–704 (2000).
44. Sengoku, T., Nureki, O., Nakamura, A., Kobayashi, S. & Yokoyama, S. Structural basis for RNA unwinding by the DEAD-box protein *Drosophila* Vasa. *Cell* **125,** 287–300 (2006).
45. Thomä, N. H. *et al.* Structure of the SWI2/SNF2 chromatin-remodeling domain of eukaryotic Rad54. *Nature Struct. Mol. Biol.* **12,** 350–356 (2005).
46. Hauk, G., McKnight, J. N., Nodelman, I. M. & Bowman, G. D. The chromodomains of the Chd1 chromatin remodeler regulate DNA access to the ATPase motor. *Mol. Cell* **39,** 711–723 (2010).
47. Zuker, M. & Stiegler, P. Optimal computer folding of large RNA sequences using thermodynamics and auxiliary information. *Nucleic Acids Res.* **9,** 133–148 (1981).
48. Gruber, A. R., Lorenz, R., Bernhart, S. H., Neubock, R. & Hofacker, I. L. The Vienna RNA websuite. *Nucleic Acids Res.* **36,** W70–W74 (2008).
49. Wan, Y., Kertesz, M., Spitale, R. C., Segal, E. & Chang, H. Y. Understanding the transcriptome through RNA structure. *Nature Rev. Genet.* **12,** 641–655 (2011).
50. Fu, X. M., Yao, Y. J., Yang, Z., Xiang, L. & Gao, J. [Alteration and its significance to expression of aquaporin-4 in cultured neonatal rat astrocytes in the model of hypoxic damage.] *Sichuan Da Xue Xue Bao Yi Xue Ban* **36,** 641–644 (2005).
51. Yang, J. *et al.* C-reactive protein augments hypoxia-induced apoptosis through mitochondrion-dependent pathway in cardiac myocytes. *Mol. Cell. Biochem.* **310,** 215–226 (2008).

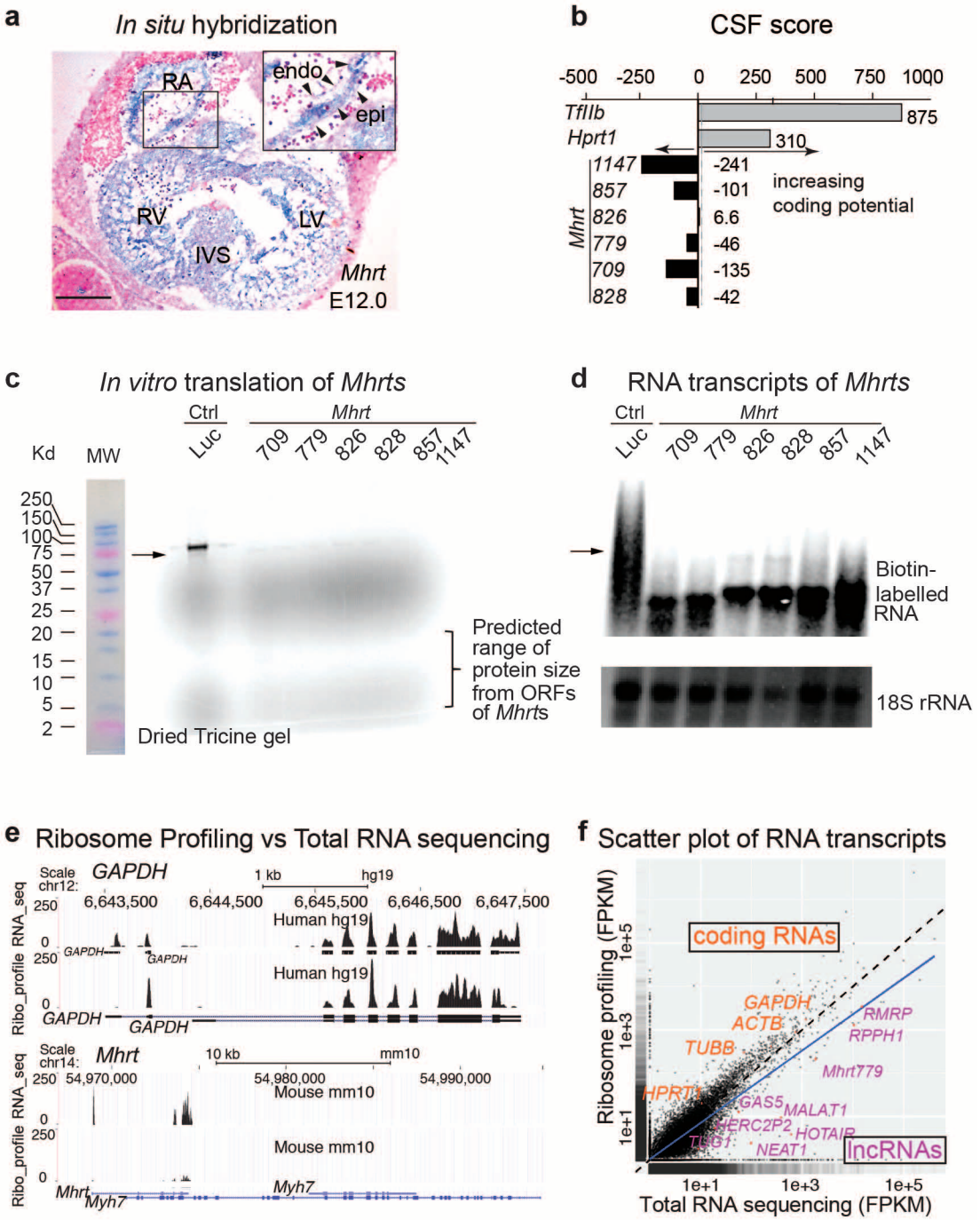

Extended Data Figure 1 | *Mhrt* RNAs have no coding potential. **a**, RNA *in situ* analysis of *Mhrt* (blue) in a mouse E12 heart. The RNA probe targets all *Mhrt* species. Red: nuclear fast red. Black arrowheads indicate nuclei of endothelial, endocardial or epicardial cells. Inset shows magnified region from the boxed area. endo, endocardium; epi, epicardium; IVS, interventricular septum; LV, left ventricle; RA and RV, right atrium and ventricle, respectively. Scale bars = 100 μm. **b**, Codon substitution frequency (CSF) scores of *Tfl1b* and *Hprt1* mRNA, as well as full-length *Mhrt* species. **c**, *In vitro* translation of control *Mhrt* species (709, 779, 826, 828, 857, 1147) and luciferase (Luc). Arrow points to the protein product of luciferase. **d**, Biotin-labelling of *Mhrt* species (709, 779, 826, 828, 857, 1147) and luciferase in the *in vitro* translation reactions. Arrow points to the RNA product of luciferase. **e**, Ribosome profiling relative to whole transcriptome RNA sequencing. *x*-axis: genomic position at the human *GAPDH* and the murine *Myh7* loci. *y*-axis: mapped reads. **f**, Scatter plot of RNA in fragments per kilobase per million reads (FPKM). Noncoding RNAs (purple) cluster towards the *x*-axis; coding RNAs (orange) towards the *y*-axis. *Mhrt779* is found below both the identity line (dashed, slope = 1, intercept = 0) and the smooth-fit regression line (in blue). RNA examples are endogenous except that *HOTAIR* was co-transfected with *Mhrt779*.

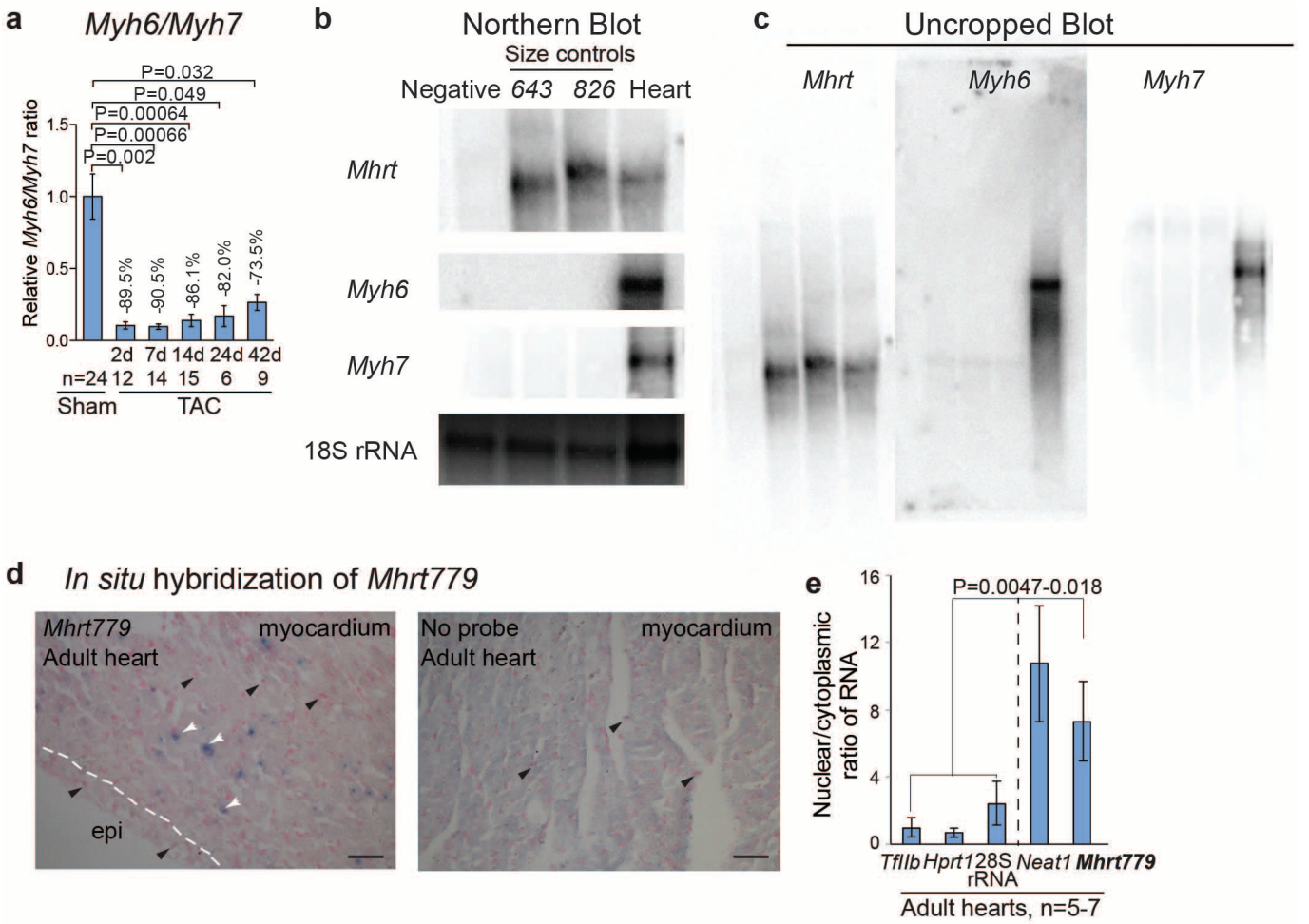

Extended Data Figure 2 | Quantification of *Myh6/Myh7*, northern blot, and *Mhrt779* characterization. **a**, Quantification of cardiac *Myh6/Myh7* ratio 2–42 days after sham or TAC operation. **b**, Northern blot analysis of *Mhrt*, *Myh6* and *Myh7*. Negative: control RNA from 293T cells. Size control: *826* is recombinant *Mhrt826*; *643* (not a distinct *Mhrt* species) contains the 5′ common region of *Mhrt*. Heart: adult heart ventricles. **c**, Un-cropped northern blots of *Mhrt*, *Myh6* and *Myh7*. **d**, RNA *in situ* hybridization of *Mhrt779* of adult heart ventricles. White arrowheads indicate nuclei of myocardial cells. Black arrowheads indicate nuclei of endothelial, endocardial or epicardial cells. Blue: *Mhrt779*; Red: nuclear fast red. Epi, epicardium. The dashed line separates the epicardium from myocardium. Scale bars = 50 μm. **e**, Quantification of *TfIIb*, *Hprt1*, 28S rRNA, *Neat1* and *Mhrt779* in the nuclear and cytoplasmic fraction of adult heart ventricle extracts. The nuclear/cytoplasmic ratio of *TfIIb* is set as 1. *P* values: Student's *t*-test. Error bars show s.e.m.

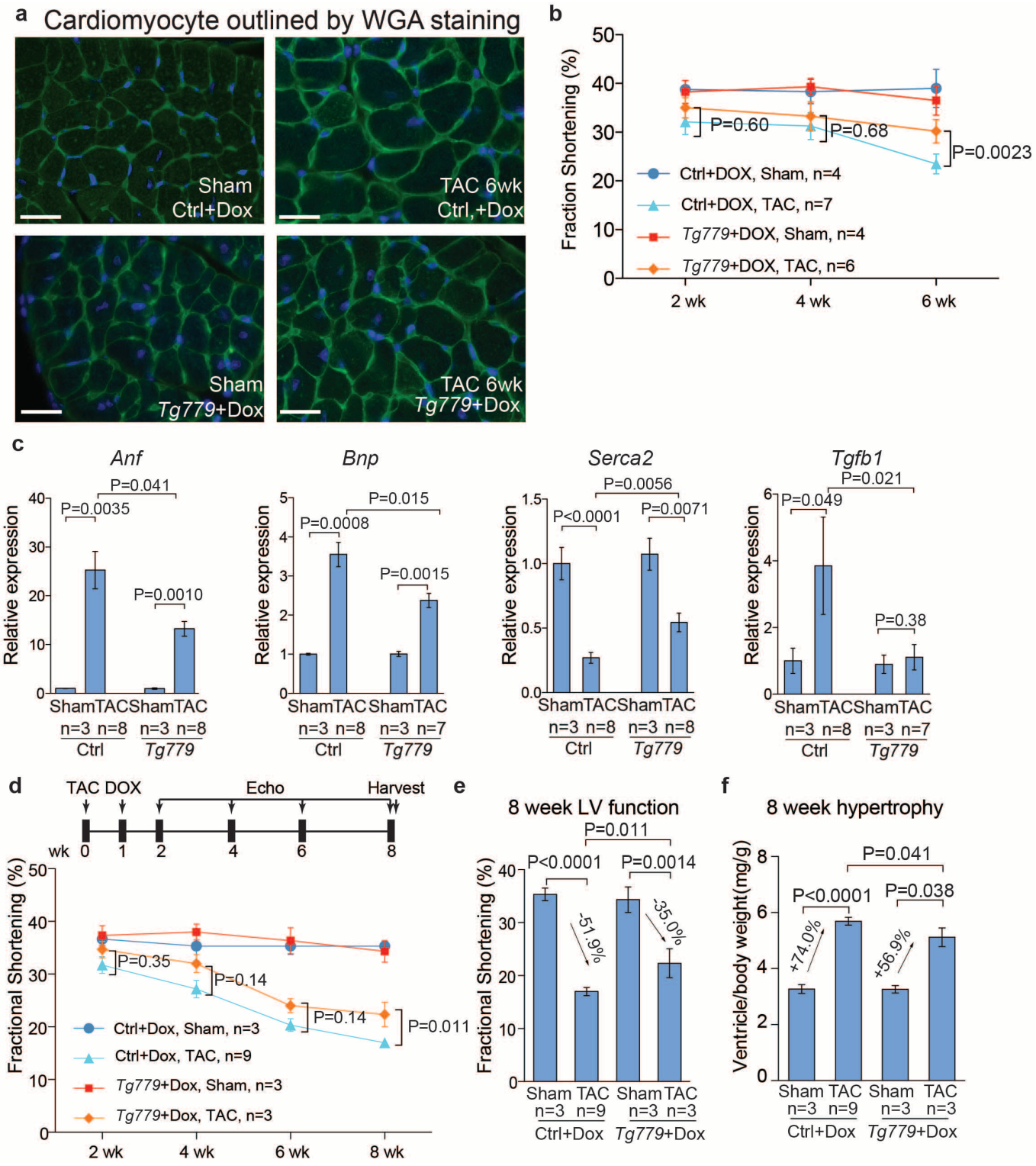

Extended Data Figure 3 | Wheat germ agglutinin staining, time course and molecular marker studies of the stressed *Tg779* mice. **a**, Wheat germ agglutinin (WGA) immunostaining 6 weeks after the sham or TAC operation. Green: WGA stain, outlining cell borders of cardiomyocytes. Blue: 4′,6-diamidino-2-phenylindole (DAPI). Ctrl, control mice. Scale bars = 50 μm. **b**, Time course of fractional shortening (FS) in control and *Tg779* mice. **c**, Quantification of *Anf*, *Bnp*, *Serca2* and *Tgfb1* in control and *Tg779* mice 2 weeks after sham or TAC operation. **d**, Experimental design for treatment study and time course of left ventricular fractional shortening changes. **e**, Fractional shortening of the left ventricle (LV) 8 weeks after the operation. **f**, Ventricular weight/body weight ratio of hearts harvested 8 weeks after sham or TAC operation. *P* values: Student's *t*-test. Error bars show s.e.m.

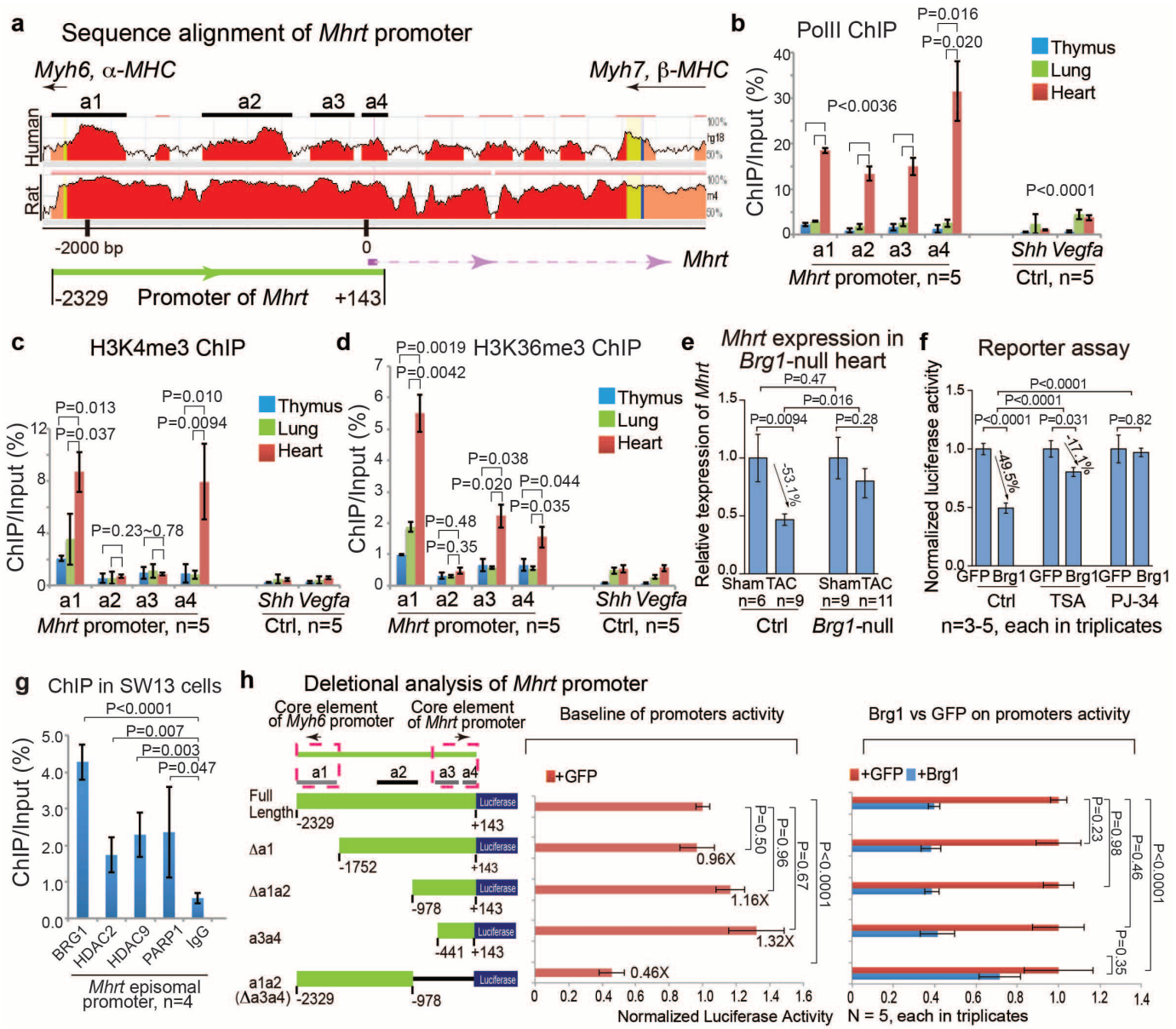

Extended Data Figure 4 | Regulation of the *Mhrt* promoter. **a**, Sequence alignment of *Mhrt* promoter loci from mouse, human and rat. Peak heights indicate degree of sequence homology. Black boxes (a1–a4) are sequences of high homology, which were used for further ChIP analysis. Green box region between *Myh6* and *Mhrt* is the putative *Mhrt* promoter. Red, promoter regions; salmon, introns; yellow, untranslated regions. **b**–**d**, ChIP–qPCR analysis of *Mhrt* promoter using antibodies against Pol II (**b**), H3K4me3 (**c**), and H3K36me3 (**d**) in tissues of adult mice. **e**, RT–qPCR quantification of *Mhrt* in control and *Brg1*-null hearts after 7 days of TAC. Ctrl, control. *Brg1*-null, *Tnnt2-rtTA;Tre-Cre;Brg1*$^{fl/fl}$. **f**, Luciferase reporter assay of *Mhrt* promoter in SW13 cells. Ctrl: dimethylsulphoxide (DMSO). PJ-34, PARP inhibitor; TSA, trichostatin (HDAC inhibitor). **g**, ChIP analysis of BRG1, HDAC2, HDAC9 and PARP1 in SW13 cells. The cells were transfected with episomal *Mhrt* promoter cloned in pREP4. **h**, Deletional analyses of the *Mhrt* promoter in luciferase reporter assays in SW13 cells. Luciferase activity of full-length *Mhrt* promoter was set up as 1. *P* values: Student's *t*-test. Error bars show s.e.m.

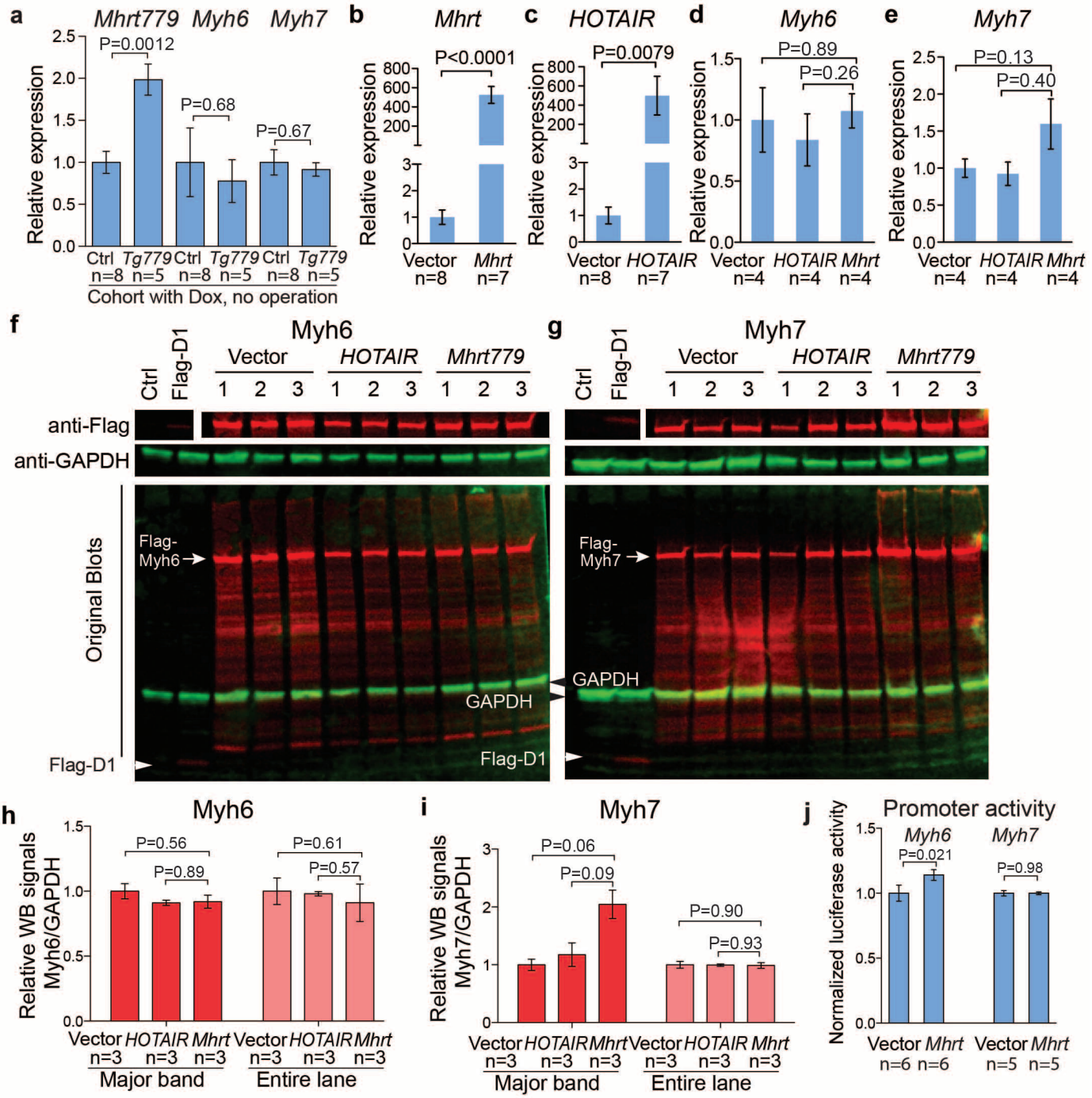

Extended Data Figure 5 | *Mhrt* does not affect *Myh* expression by direct RNA sequence interference. **a**, qPCR analysis of *Mhrt779*, *Myh6* and *Myh7* in mice without TAC operation. Expression levels were normalized to *TfIIb*, and the control is set as 1. Ctrl, control mice. **b**, **c**, RNA quantification of *Mhrt* (**b**) and *HOTAIR* (**c**) in SW13 cells transfected with Vector (pAdd2), *HOTAIR* (pAdd2-*HOTAIR*) or *Mhrt* (pAdd2-*Mhrt779*). Expression in vector-transfected cells is set as 1. Constructs containing *Myh6* or *Myh7* were co-transfected into SW13 cells used for Fig. 2b–i. **d**, **e**, RNA quantification of *Myh6* (**d**) and *Myh7* (**e**) in SW13 cells relative to *GAPDH*. **f**, **g**, Western blot analysis of Myh6 (**f**) and Myh7 (**g**) in SW13 cells. Constructs containing *Myh6*- and *Myh7*-coding sequences were tagged with Flag and co-transfected with vector, *HOTAIR* or *Mhrt779*. GAPDH was used as the loading control. Flag–D1 was used as a positive control for the Flag antibody. **h**, **i**, Protein quantification of Myh6 (**h**) and Myh7 (**i**) in control and transfected SW13 cells relative to GAPDH. Signals of Myh6 and Myh7 from major bands or the entire lanes were quantified.WB, western blot. **j**, Luciferase reporter assay of *Mhy6* and *Myh7* promoters in SW13 cells transfected with vector (pAdd2) or *Mhrt* (pAdd2-*Mhrt779*). *P* values: Student's *t*-test. Error bars show s.e.m.

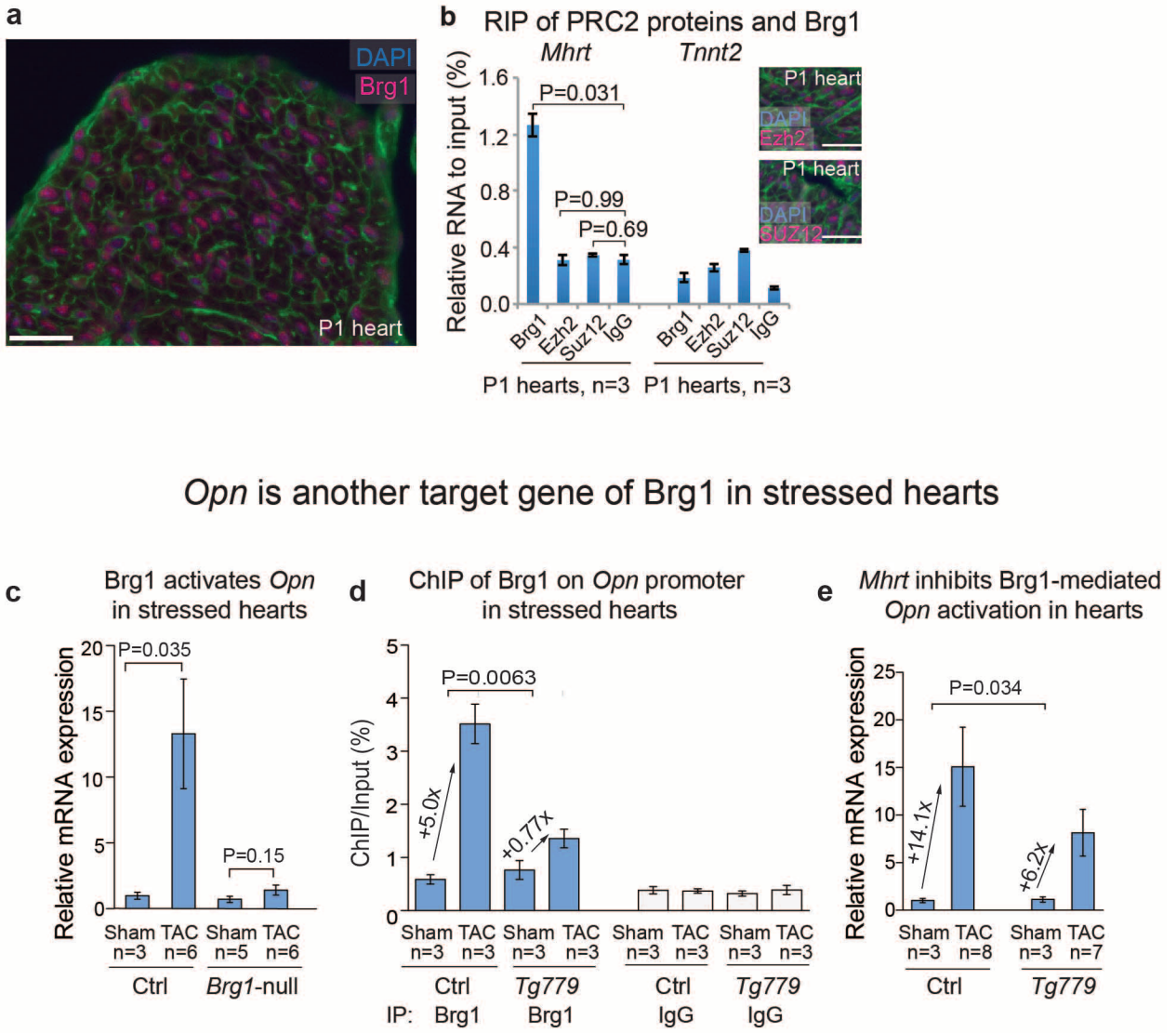

Extended Data Figure 6 | RNA-IP controls; *Opn* is another target gene of Brg1 in stressed hearts. **a**, Immunostaining of Brg1 in P1 heart. Red: Brg1. Green: WGA. Blue: DAPI. Ctrl, control. Scale bar = 50 μm. **b**, RNA-IP of *Mhrt* in P1 hearts using antibodies against Ezh2 and Suz12. Right panels show immunostaining of Ezh2 and Suz12 in P1 hearts. PRC2, polycomb repressor complex 2. Red: Ezh2 or Suz12. Green: WGA. Blue: DAPI. Scale bars = 50 μm. **c**, Quantification of *Opn* mRNA in control and *Brg1*-null (*Tnnt2-rtTA;Tre-Cre;Brg1*$^{fl/fl}$) mice after sham or TAC operation. **d**, ChIP of Brg1 on *Opn* proximal promoter in control and transgenic (*Tg779*) mice after sham or TAC operation. **e**, Quantification of *Opn* in control and transgenic (*Tg779*) mice after sham or TAC operation. *P* values: Student's *t*-test. Error bars show s.e.m.

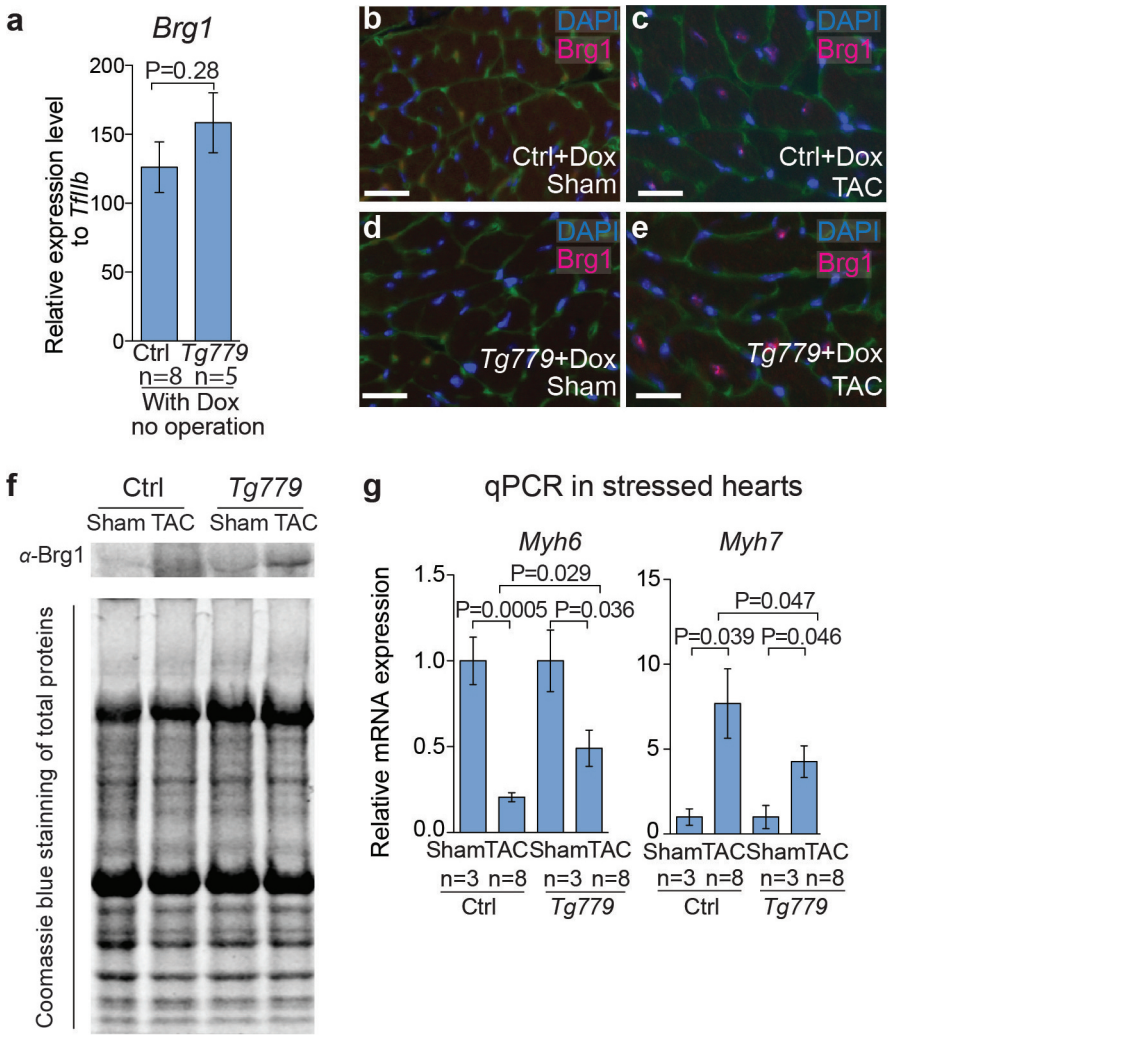

Extended Data Figure 7 | Induction of *Mhrt779* is insufficient to change Brg1 mRNA or protein level. **a**, qPCR analysis of *Brg1* expression in hearts without TAC operation. Ctrl: control mice. **b**–**e**, Immunostaining of Brg1 (red) in adult heart ventricles 2 weeks after sham or TAC operation. Green: WGA. Blue: DAPI. Scale bars = 50 μm. **f**, Western blot analysis of Brg1 and Coomassie staining of total proteins in control or *Tg779* hearts after 2 weeks of sham or TAC operation. **g**, Quantification of *Myh6* and *Myh7* in control (Ctrl) and *Tg779* hearts after 2 weeks of sham or TAC operation. *P* values: Student's *t*-test. Error bars show s.e.m.

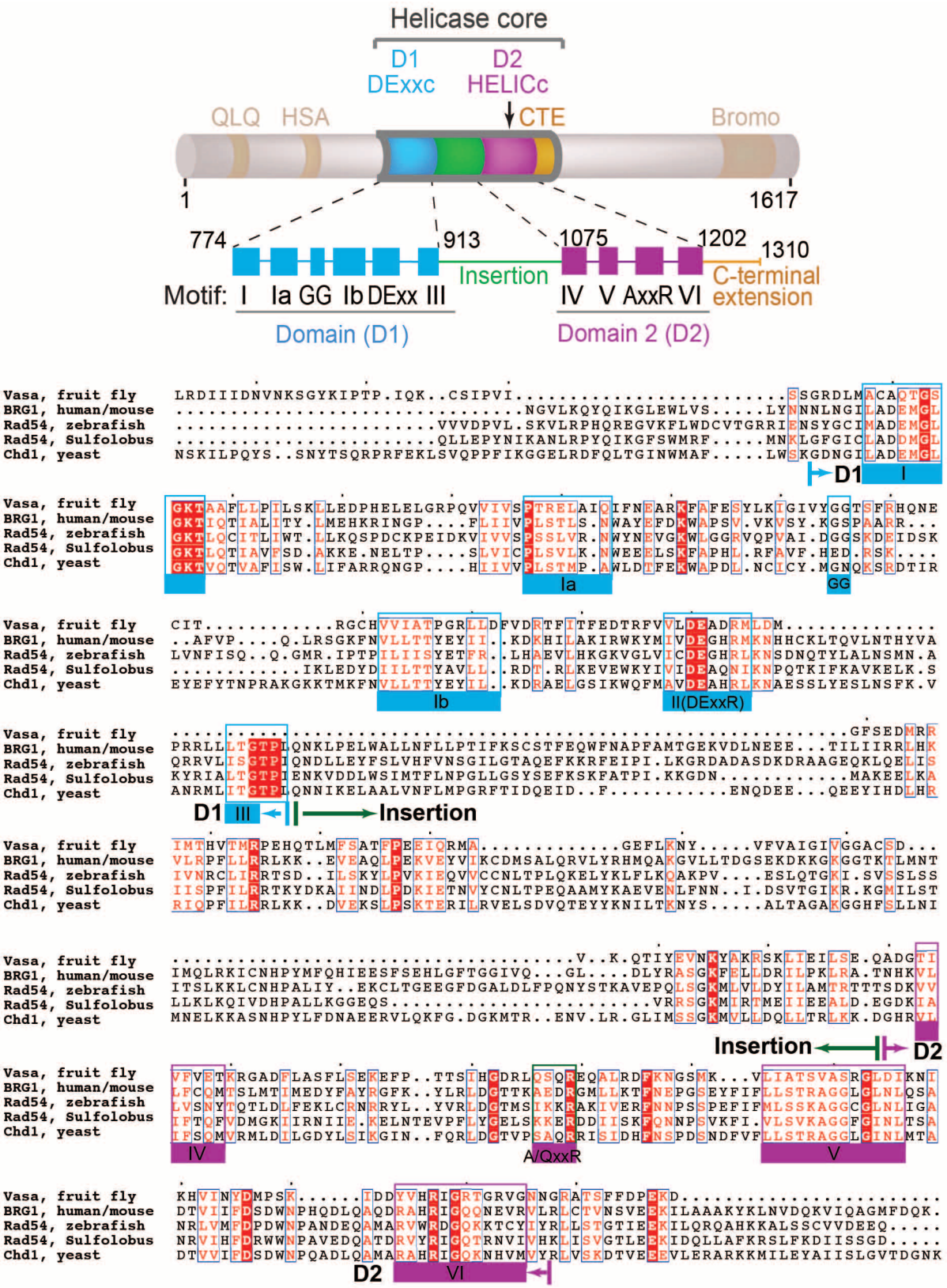

Extended Data Figure 8 | Brg1 sequence alignment and motif analysis. Schematics of the architecture of mouse Brg1 and the sequence alignment of Brg1, Vasa (fruit fly), Rad54 (zebrafish, *Sulfolobus solfataricus*) and Chd1 (yeast). The motifs were outlined by blue boxes (D1 domain) and purple boxes (D2 domain).

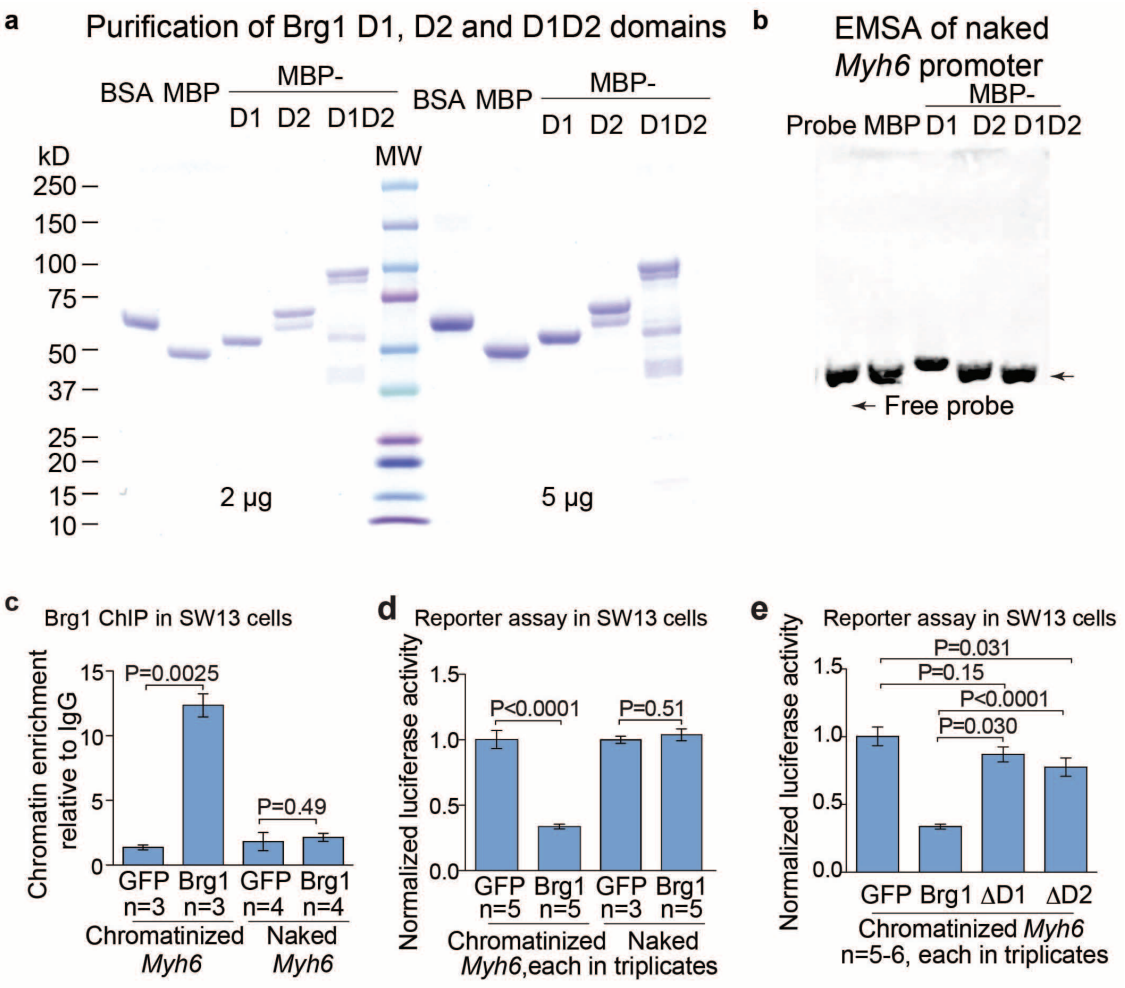

Extended Data Figure 9 | Purification of Brg1 helicase core domains, EMSA of naked *Myh6* promoter, ChIP and reporter studies in SW13 cells. **a**, Coomassie blue staining of purified MBP-tagged Brg1 helicase domains. Bovine serum albumin (BSA) was loaded as a control. **b**, EMSA assay of naked *Myh6* promoter (−426 to +170) with helicase domains of Brg1. Probe: biotin-labelled *Myh6* promoter. 50 µM of MBP, MBP–D1, MBP–D2 and MBP–D1D2 proteins were used for EMSA. **c**, **d**, ChIP (**c**) and luciferase reporter (**d**) analysis of Brg1 on chromatinized (episomal) and naked *Myh6* promoter in SW13 cells. GFP, green fluorescent protein control. **e**, The luciferase reporter of helicase-deficient Brg1 on chromatinized (episomal) *Myh6* promoter in SW13 cells. ΔD1: Brg1 lacking amino acids 774–913. ΔD2: Brg1 lacking amino acids 1086–1246. ChIP: H-10 antibody recognizing N terminus, non-disrupted region of Brg1. *P* values: Student's *t*-test. Error bars show s.e.m.

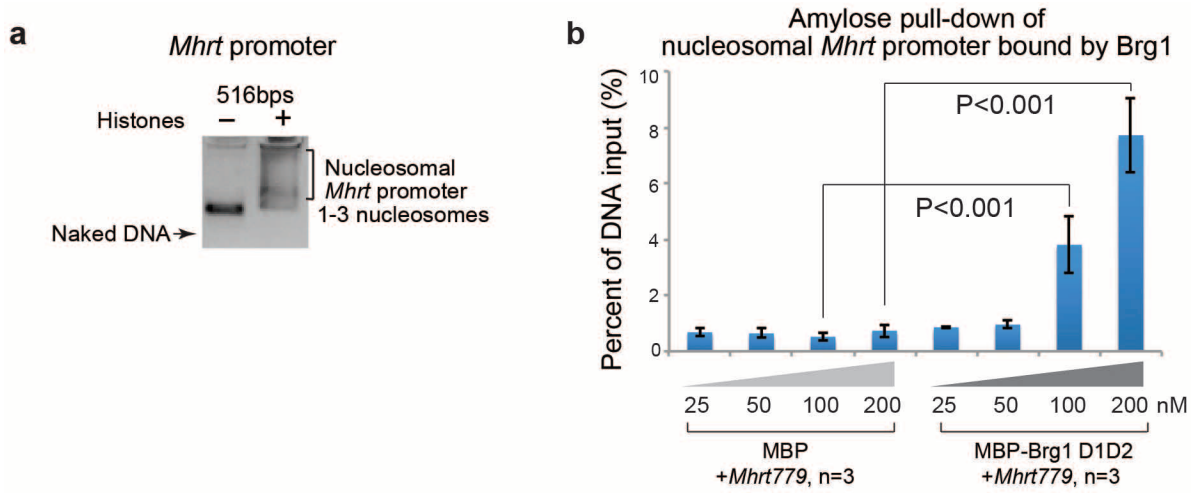

Extended Data Figure 10 | Brg1 outruns *Mhrt* to bind to its target *Mhrt* promoter. **a**, Assembly of nucleosomes on the *Mhrt* promoter (a3/4). **b**, Amylose pull-down assay: amylose was used to pull down the chromatinized *Mhrt* promoter that was incubated with various doses of MBP and MBP–Brg1 D1D2. DNA precipitated by amylose was further quantified by qPCR. *P* values: Student's *t*-test. Error bars show s.e.m.

a Sequence alignment of human and mouse *MyHEART*

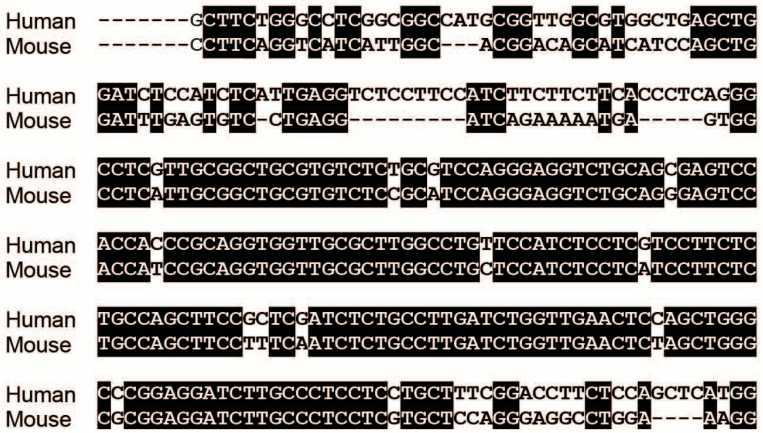

b Predicted secondary strucutre of human and mouse *MyHEART*

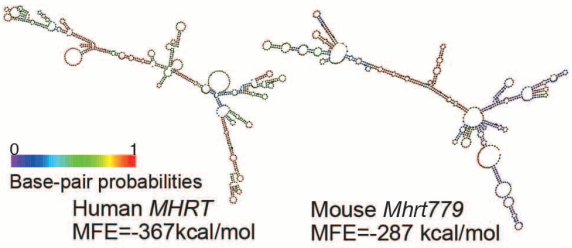

c Demography of human subjects

Control individuals with normal hearts

Age	Gender	Clinical diagnosis
38	M	Normal LV thickness and function
49	M	Normal LV thickness and function
42	F	Normal LV thickness and function
31	M	Normal LV thickness and function

*LVH: left ventricular hypertrophy.
+ICM: ischemic cardiomyopathy.
#IDCM: idiopathic dilated cardiomyopathy

Patients with cardiomyopathy

Age	Gender	Clinical diagnosis
49	M	LVH*
46	M	LVH
28	F	LVH
48	M	LVH
39	M	LVH
59	M	ICM+
58	M	ICM
57	M	ICM
59	F	IDCM#
59	M	IDCM
56	M	IDCM
51	F	IDCM
35	F	IDCM
54	F	IDCM

Extended Data Figure 11 | Sequence alignment and secondary structure prediction of human and mouse *MHRT*, and demography of heart transplantation donors. **a**, Sequence alignment of human *MHRT* and mouse *Mhrt779*. **b**, Predicted secondary structure of mouse *Mhrt779* and human *MHRT*, using minimal free energy (MFE) calculation of RNAfold WebServer. **c**, Demography of human subjects whose tissues were used for RT–qPCR analysis (Fig. 4l). ICM, ischaemic cardiomyopathy; IDCM, idiopathic cardiomyopathy; LVH, left ventricular hypertrophy.